



Simplified mantle architecture and distribution of radiogenic power

Ricardo Arevalo Jr.

*Planetary Environments Lab, NASA Goddard Space Flight Center, Greenbelt, Maryland, USA
(ricardo.d.arevalo@nasa.gov)*

William F. McDonough

Department of Geology, University of Maryland, College Park, Maryland, USA

Andreas Stracke

Institut für Mineralogie, Westfälische Wilhelms Universität Münster, Munster, Germany

Matthias Willbold

School of Earth Sciences, University of Bristol, Bristol, UK

Thomas J. Ireland

Department of Earth Sciences, Boston University, Boston, Massachusetts, USA

Richard J. Walker

Department of Geology, University of Maryland, College Park, Maryland, USA

[1] The mantle components that represent the source region of ocean island basalts (OIB) and feed hotspot volcanism are predicted to contain 160 ± 20 ($2\sigma_m$) ng/g Th, a heat-producing element. This critical model composition indicates that the OIB source region (OSR) comprises a significant amount of recycled oceanic crust and constitutes 19^{+3}_{-2} ($2\sigma_m$)% of the mantle by mass. The mass fraction of this reservoir supports a mantle architecture with a basal thermochemical layering at an average depth of 2000 ± 100 ($2\sigma_m$) km or two thermochemical piles that extend up to midmantle levels. The hotspot source described here generates 10 pW/kg of radiogenic heat and supplies 7.3 TW to the planet's total surface heat flux. Given that the silicate portion of the Earth produces some 20.4 TW of radiogenic power, with 7.2 TW derived from the continental crust, the mantle source responsible for mid-ocean ridge volcanism provides only 5.9 TW of radiogenic power (or <2 pW/kg). As a result, the source of hotspots generates $>5x$ more radiogenic heat than the source of mid-ocean ridges, thus contributing to the energetics that drive mantle convection and potentially the formation of long-lived plumes via bottom heating of the modern mantle. The potential for a sequestered or unsampled mantle reservoir would impact the relative mass fractions of the source regions of OIB and mid-ocean ridge volcanism but not the compositional model of the OSR presented here.

Components: 10,963 words, 7 figures, 6 tables.

Keywords: OIB; mantle; hotspot; source; radiogenic heat; mass balance.

Index Terms: 1025 Composition of the mantle: Geochemistry; 1038 Mantle processes: Geochemistry; 1065 Major and trace element geochemistry: Geochemistry; 1009 Geochemical modeling: Geochemistry; 3610 Geochemical modeling: Mineralogy and Petrology; 3621 Mantle processes: Mineralogy and Petrology; 8410 Geochemical modeling: Volcanology.

Received 17 January 2013; **Revised** 10 April 2013; **Accepted** 12 April 2013; **Published** 29 July 2013.



Arevalo, R., Jr., W. F. McDonough, A. Stracke, M. Willbold, T. J. Ireland, and R. J. Walker (2013), Simplified mantle architecture and distribution of radiogenic power, *Geochem. Geophys. Geosyst.*, 14, 2265–2285, doi:10.1002/ggge.20152.

1. Introduction

[2] The silicate portion of the Earth may be quantitatively defined by the continental crust (CC) and subcontinental lithospheric mantle, the mantle reservoir that produces mid-ocean ridge basalts (MORB), and the mantle source(s) that contribute to the generation of intraplate ocean island basalts (OIB). However, our understanding of the mantle's architecture remains poorly constrained. Geochemical and geophysical perspectives of mantle structure differ due to the inherent inconsistencies between what is measured in samples collected at the surface and what is modeled in the planet's interior. Geochemical studies require a multicomponent mantle and have traditionally favored a compositionally layered mantle structure in order to account for:

[3] (1) The scale of elemental and isotopic heterogeneity observed in oceanic basalts and the distinct compositional characteristics associated with basalts derived from mid-ocean ridges versus those from intraplate hotspot sources [e.g., DePaolo and Wasserburg, 1976; O'Nions et al., 1979; Allègre et al., 1979];

[4] (2) Noble gas isotopic compositions, including He, Ne, Ar, and Xe, as measured in intraplate volcanics [e.g., Kurz et al., 1982; Allègre et al., 1983; Honda et al., 1991];

[5] (3) Geochemical and cosmochemical evidence for a “hidden” or unsampled mantle reservoir from trace element abundances [e.g., Rudnick et al., 2000], ¹⁴⁶Sm-¹⁴²Nd isotopes [e.g., Boyet and Carlson, 2005] and rare gas systematics [e.g., Tolstikhin and Hofmann, 2005];

[6] (4) The mass balance of radiogenic heat production in the silicate portion of the Earth [e.g., Turcotte et al., 2001; van Keken et al., 2002; Jau-part et al., 2007; Arevalo et al., 2009].

[7] Conversely, geophysical models implicate a well-mixed mantle based on seismic evidence for mass flux/exchange across the transition zone and as deep as the core-mantle boundary [e.g., Grand, 1994; van der Hilst et al., 1997; Ritsema et al., 1999; Zhao, 2001; Montelli et al., 2004]. Observations based on mantle seismicity also suggest

significant lower mantle structure, as manifested by slow seismic anomalies identified beneath the central Pacific Ocean and southern Africa [e.g., Su et al., 1994; Breger and Romanowicz, 1998; Wang and Wen, 2004]; ubiquitous compositional and/or thermal heterogeneity in the deepest 1000 km of the mantle [e.g., van der Hilst and Kárason, 1999; Garnero, 2000; Trampert et al., 2004]; and a variety of slab behaviors across the global transition zone [e.g., Kárason and van der Hilst, 2000; Fukao et al., 2001; Grand, 2002], including lithospheric slabs that appear to be locally inhibited from penetrating the 660 km discontinuity [e.g., Zhou and Clayton, 1990; Van der Hilst et al., 1991; Fukao et al., 1992] or lose resolution at midmantle depths [e.g., Wen and Anderson, 1995; van der Hilst et al., 1997; Ritsema et al., 2004]. As a result, traditional models of a strictly layered or uniform mantle architecture do not adequately satisfy all multidisciplinary requirements, and thus an alternative model of mantle structure is needed to reconcile all of the above observations.

[8] Based on seismological, dynamical, and chemical arguments, a number of hybrid models of mantle structure have been proposed in an attempt to unite both geochemical and geophysical observations. Notably, several studies [e.g., Wen and Anderson, 1995; Kellogg et al., 1999; van der Hilst and Kárason, 1999; Anderson, 2002] have invoked a rendition of the stratified mantle paradigm, but with a diffuse, midmantle (e.g., ≥ 1000 km average depth) chemical boundary layer with substantial surface topography, a feature that is consistent with laboratory experiments of thermochemical convection in a fluid with stratified density and viscosity [e.g., Davaille, 1999; Davaille et al., 2003] and could explain the lack of unequivocal seismic evidence for this layering. The existence of large, low-shear velocity provinces in the lower mantle, commonly termed “superswells” or “superplumes,” beneath the central Pacific Ocean and southern Africa [e.g., Su et al., 1994; Breger and Romanowicz, 1998; Wang and Wen, 2004], may represent the manifestation of this midmantle chemical boundary layer in the form of isolated thermochemical “piles” of material that may extend up to ~ 1500 km from the core-mantle boundary [e.g., Tackley, 1998; Ni et al., 2002; McNamara and Zhong, 2005]. However, direct



evidence for this proposed midmantle thermochemical boundary layer has yet to be unambiguously identified [e.g., *Masters et al.*, 2000; *Vidale et al.*, 2001]

[9] The existence of multiple distinct mantle source regions has important mass balance implications for paradigms of modern mantle structure. Mid-ocean ridge basalts, which are derived from an upper mantle source (i.e., <200 km depth) [e.g., *Forsyth et al.*, 1998], exhibit only limited ranges in radiogenic isotopic signatures (e.g., ⁸⁷Sr/⁸⁶Sr, ¹⁴³Nd/¹⁴⁴Nd, etc.) and are largely depleted in incompatible elements (i.e., $D_i^{\text{sol/liq}} < 1$, where D is approximated by the concentration ratio of element i in the solid to the liquid). Intraplate OIB, on the other hand, commonly sample one or more discrete deep-rooted hotspot sources (i.e., >660 km depth) [e.g., *Montelli et al.*, 2004], span a significantly wider range of radiogenic isotopic signatures [e.g., *Zindler and Hart*, 1986], and tend to be enriched in incompatible elements [e.g., *Sun and McDonough*, 1989]. Although models inevitably vary due to sampling biases and differences in the statistical treatment of data, the chemical composition of the MORB source region has been well characterized due to the extensive number of submarine and dredge basalts available for analysis. In comparison, the source regions of OIB remain relatively unconstrained due to fewer samples available for chemical analysis at many OIB localities, greater diversity in trace element and isotopic signatures compared to MORB, and challenges/uncertainties in establishing near-primary (or parental) melt compositions.

[10] Mass balance in the silicate portion of the Earth obeys the following relationship:

$$M^{\text{BSE}} X_i^{\text{BSE}} = M^{\text{CL}} X_i^{\text{CL}} + M^{\text{DMM}} X_i^{\text{DMM}} + M^{\text{OSR1}} X_i^{\text{OSR1}} + M^{\text{OSR2}} X_i^{\text{OSR2}} + \dots, \quad (1)$$

where M represents the mass (in g) and X_i the abundance (in μg/g) of element i in the bulk silicate earth (BSE), continental lithosphere (CL; including the crust and subcontinental lithospheric mantle), depleted MORB mantle (DMM), and discrete OIB source regions (OSR1, OSR2, etc.). There are a variety of compositional models of the BSE, CL, and DMM, but representative compositions of OSR have never been established. Further, although the masses of the BSE and CL are well constrained [e.g., *Yoder*, 1995], the relative fractions of the modern mantle that are represented by the DMM and OSR(s) remain poorly constrained. Here, we

present a geochemical model that estimates the chemical enrichment of the sources of a collection of OIB (Figure 1), including alkalic lavas derived from both high μ (HIMU; where $\mu = (^{238}\text{U}/^{204}\text{Pb})_{t=0}$) and enriched mantle (EM) “end-member”-type sources [e.g., *Zindler and Hart*, 1986], and we explore the implications of this model mantle composition with regard to the mass balance of highly incompatible elements (i.e., $D_i^{\text{sol/liq}} \ll 1$), including heat-producing K, Th, and U.

[11] The model presented here is based on determining the abundances of Th in near-primary parental melts from a variety of OIB end-member localities, including HIMU-type Cook-Austral and St. Helena islands; EM(I)-type Heard, Tristan da Cunha, Gough, and Pitcairn islands; EM(II)-type Marquesas, Azores, Society, and Samoa islands; and for comparison, Hawaii, Galapagos, and Iceland, which produce dominantly tholeiitic volcanic products and generally do not record extreme radiogenic isotopic signatures (Figure 1). With regard to incompatible elements, the parental melt compositions established here are based on bivariate linear regression trends between the MgO contents of the lavas considered and their respective abundances of Th, the most highly incompatible element that is neither fluid mobile, such as the large-ion lithophile elements (e.g., K, Rb, Cs, Ba), nor sensitive to redox conditions, as for example multivalent W and U. The abundances of highly incompatible elements, particularly those with radioactive isotopes such as K, Th and U, in the sources of these hotspot basalts provide a unique geochemical window into the spatial and compositional characteristics of a potentially common OSR, including its size, chemical enrichment, and rate of radiogenic heat production.

2. OIB Source Characteristics

[12] The degree of heterogeneity observed in global OIB (Figure 1) has traditionally been interpreted to represent mixing between a finite number of mantle “end-members,” as defined by isotopic distinctions [e.g., *White*, 1985; *Zindler and Hart*, 1986] and trace element signatures [e.g., *Sun and McDonough*, 1989; *Weaver*, 1991]. However, some geochemical attributes are shared between the different flavors of OIB. Although exceptions occur, OIB are characterized commonly by (1) superprimitive (i.e., enriched relative to the unfractionated BSE) U/Pb, Th/Pb, and U/Th, and subprimitive Rb/Sr and Nd/Sm ratios [e.g., *Gast et*

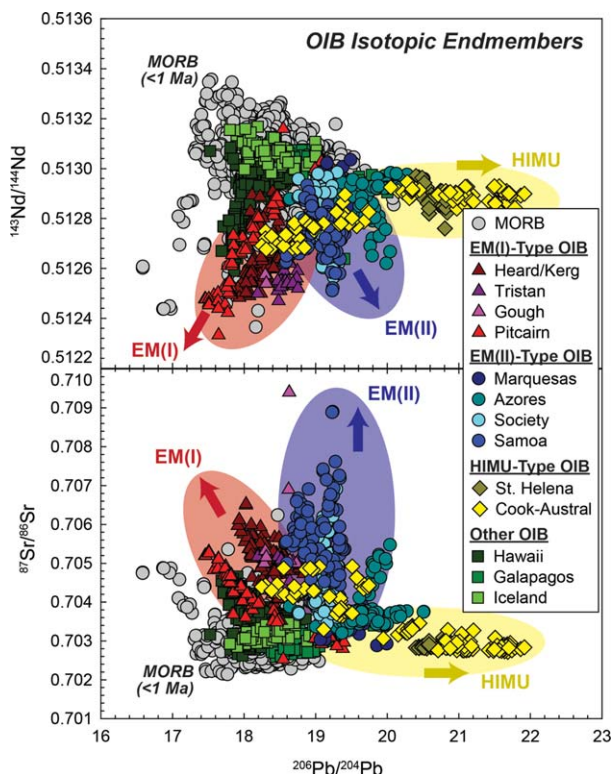


Figure 1. Published isotopic compositions of lavas derived from the OIB localities examined in this study. Data compiled by *Stracke et al.* [2003]. The degree of heterogeneity observed in the radiogenic isotopic compositions of global OIB has historically been interpreted to represent mixing between a finite number of mantle components, including HIMU- (where $\mu = (^{238}\text{U}/^{204}\text{Pb})_{t=0}$) and EM-type “end-members” [e.g., *White*, 1985; *Zindler and Hart*, 1986]. Volcanics derived from EM-type sources are often categorized into EM(I)- and EM(II)-type lavas (as shown above), though this division is rather arbitrary and unsupported by trace element systematics [*Willbold and Stracke*, 2006].

al., 1964; *Gast*, 1968; *Schilling*, 1973; *DePaolo and Wasserberg*, 1976; *Tatsumoto*, 1978]; (2) superprimitive Nb/U and Ce/Pb ratios, similar to MORB but opposite the subprimitive values observed in the continental crust [e.g., *Hofmann et al.*, 1986]; (3) more highly radiogenic Pb than the BSE [e.g., *Gast et al.*, 1964; *Allègre*, 1968; *Tatsumoto*, 1978]; (4) systematically higher $^{87}\text{Sr}/^{86}\text{Sr}$ and $^3\text{He}/^4\text{He}$, lower $^{143}\text{Nd}/^{144}\text{Nd}$ and $^{176}\text{Hf}/^{177}\text{Hf}$, and more extreme values in $^{206}\text{Pb}/^{204}\text{Pb}$, $^{207}\text{Pb}/^{204}\text{Pb}$, and $^{208}\text{Pb}/^{204}\text{Pb}$ compared to MORB [e.g., *Allègre et al.*, 1983; *Zindler et al.*, 1982; *Zindler and Hart*, 1986; *Hofmann*, 2003; *Stracke et al.*, 2005 and references therein]; and (5) observed abundances of incompatible elements that are too enriched to be accounted for by conventional melting of an undifferentiated source

without requiring unrealistically small degrees of partial melting (e.g., $F \leq 1\%$) [*Hofmann and White*, 1982; *Hofmann*, 1988; *Sun and McDonough*, 1989].

[13] Further, HIMU-type (e.g., St. Helena) and EM-type (e.g., Gough Island) OIB exhibit a number of robust compositional similarities [*Willbold and Stracke*, 2006], including enrichments in light rare earth element (LREE) abundances relative to average chondritic meteorites (CI) and the BSE; depletions in heavy rare earth elements relative to LREE concentrations; and comparable ratios of La/Th, Sr/Nd and alkali-to-alkaline earth elements (e.g., Rb/K, Ba/K, etc.). These mutual geochemical attributes likely reflect similar source compositions and/or a common source component, most likely recycled oceanic lithosphere. However, a number of alternative models have also been postulated for the origin of OIB, including (1) linear mixing of four end-member components in the deep mantle [e.g., *Hart*, 1988]; (2) partial or complete melting of deep, metasomatized portions of oceanic peridotite [*Niu and O’Hara*, 2003]; and/or (3) deep melting of small amounts of recycled mafic crust [e.g., *Prytulak and Elliott*, 2007]. Here, we attempt to model the incompatible trace element budget of OIB sources by estimating near-primary parental melt compositions based on systematic geochemical variations (i.e., Th versus MgO) in basalts from several key OIB localities, namely, HIMU-type Cook-Austral and St. Helena islands; EM(I)-type Heard, Tristan da Cunha, Gough, and Pitcairn islands; EM(II)-type Marquesas, Azores, Society, and Samoa islands; and for comparison, Hawaii, Galapagos, and Iceland.

3. Estimating OIB Near-Primary Parental Melt Compositions

[14] Here we evaluate major element and incompatible trace element abundances for OIB derived from the hotspot localities listed above, including a new high-quality data set for the HIMU-type Cook-Austral Islands (Table 1); see *Willbold and Jochum* [2005] and *Willbold and Stracke* [2006] for details on the specific methodology, including procedures, analyses of reference materials, and measurements of accuracy and reproducibility. Representative published data sets have also been compiled for HIMU-type St. Helena; EM(I)-type Heard, Tristan da Cunha, Gough, and Pitcairn islands; EM(II)-type Marquesas, Azores, Society, and Samoa islands; and, Hawaii, Galapagos, and Iceland. Only data sets derived from single



Table 1. Major (in wt.%) and Incompatible Trace Element (in µg/g) Abundances Measured in Oceanic Basalts from the HIMU-Type Cook-Austral Islands

Sample	SiO ₂	Al ₂ O ₃	Fe ₂ O ₃	FeO	MnO	MgO	CaO	Na ₂ O	K ₂ O	TiO ₂	P ₂ O ₅	Total	Mg#	Th	U	Nd	Sm	Refs
Mangaia																		
MGA02	43.6	11.2	2.21	11.3	0.18	10.8	11.5	2.07	0.70	2.86	0.45	96.8	63.1	3.28	0.931	33.1	6.67	[1]
MGA10	44.0	10.1	2.10	10.7	0.19	12.7	11.8	1.49	0.45	2.67	0.42	96.6	67.9	4.38	1.169	37.8	7.39	[1]
MGA103	43.4	13.3	2.15	10.9	0.21	9.0	12.0	2.32	0.84	2.88	0.53	97.5	59.4	4.33	1.162	40.1	7.82	[1]
MGA105	43.0	13.5	2.44	12.4	0.22	6.1	12.3	2.69	0.81	3.01	0.39	96.8	46.6	3.05	0.875	33.7	7.15	[1]
MGA106	44.5	7.4	2.01	10.2	0.19	19.5	10.9	1.13	0.19	1.74	0.22	98.1	77.2	1.47	0.437	17.5	3.77	[1]
MGA108	44.7	11.2	1.95	10.0	0.19	9.6	14.4	2.50	0.60	2.52	0.36	98.0	63.3	2.73	0.774	30.3	6.28	[1]
MGA111	44.0	9.6	1.94	9.9	0.19	11.7	14.5	1.95	0.60	2.46	0.39	97.2	67.9	3.07	0.862	38.5	6.19	[1]
MGA113	43.4	8.4	2.12	10.8	0.21	17.6	11.2	1.67	0.48	1.98	0.33	98.2	74.4	2.56	0.734	25.3	5.02	[1]
MGA116	44.2	12.9	1.97	10.0	0.21	7.1	13.5	2.65	0.75	2.70	0.49	96.5	55.9	3.83	1.095	38.2	7.42	[1]
MGA117	44.4	10.6	2.02	10.3	0.20	12.7	12.2	2.74	0.67	2.18	0.40	98.4	68.8	3.08	0.829	26.5	5.28	[1]
Tubuai																		
TB15	43.0	6.6	2.01	10.3	0.20	23.0	10.0	1.32	0.40	1.44	0.19	98.4	80.0	2.58	0.579	33.6	5.94	[3]
TB35	41.5	12.3	2.30	11.7	0.26	8.2	9.2	6.10	1.51	2.83	1.05	97.0	55.5	3.67	0.930	31.8	6.31	[2]
TBA01	42.7	7.1	2.02	10.3	0.18	19.3	12.2	0.65	0.18	1.88	0.26	96.7	76.9	2.35	0.476	22.9	4.51	[2]
TBA09	42.9	10.2	2.51	12.8	0.22	17.9	8.8	0.28	0.19	2.92	0.23	98.9	71.4	4.25	1.143	40.2	7.43	[1]
TBA11	46.5	16.2	2.62	13.4	0.27	9.3	3.8	0.30	0.34	3.07	0.23	95.9	55.3	6.28	0.856	52.4	9.57	[1]
TBA16	41.5	11.0	2.22	11.3	0.19	11.6	11.9	2.58	0.77	2.88	0.58	96.5	64.6	6.52	1.553	44.4	8.11	[4]
TBA33	43.4	12.2	2.17	11.0	0.21	10.2	12.0	2.47	0.86	2.65	0.38	97.7	62.3	4.59	1.237	37.9	7.00	[3]
TBA36	44.3	9.8	1.98	10.1	0.18	13.8	11.7	1.51	0.70	2.22	0.41	96.7	70.9	3.43	0.955	31.6	6.28	[2]
TBA102	43.1	10.3	2.08	10.6	0.20	11.8	13.1	2.07	0.50	2.58	0.47	96.8	66.4	4.35	1.028	37.6	7.12	[2]
TBA109	44.0	12.0	2.19	11.2	0.21	10.0	12.0	2.22	0.72	2.76	0.42	97.8	61.5	3.54	0.941	34.2	6.82	[4]
Raivavae																		
RVV02	46.8	14.0	1.85	9.4	0.15	7.7	10.6	2.94	0.87	2.80	0.48	97.6	59.2	3.67	0.963	35.9	7.22	[1]
RVV108	50.9	14.7	1.84	9.4	0.14	5.2	9.4	3.00	0.55	2.26	0.33	97.7	49.8	1.93	0.539	22.8	5.80	[5]
RVV114	45.5	15.3	2.06	10.5	0.17	5.6	9.7	2.84	1.10	3.10	0.46	96.4	48.8	4.50	1.044	38.1	7.40	[3]
RVV123	47.6	11.6	1.93	9.8	0.15	13.2	8.9	2.35	0.46	2.19	0.31	98.5	70.4	2.00	0.402	23.3	5.31	[1]
RVV124	47.4	11.3	1.90	9.7	0.14	14.0	8.1	2.39	0.63	1.96	0.32	97.8	72.1	1.96	0.470	20.2	4.50	[2]
RVV139	44.9	10.3	2.02	10.3	0.16	15.7	10.0	2.20	0.65	2.13	0.37	98.6	73.2	3.33	0.739	31.0	5.88	[2]
Rapa																		
RA07	45.2	12.5	1.89	9.7	0.15	11.2	8.8	2.24	1.10	3.46	0.76	96.9	67.3	3.39	1.188	38.5	7.69	[2]
RA24	44.2	14.4	2.07	10.6	0.15	7.2	8.1	3.56	1.97	4.18	0.97	97.5	54.9	5.28	1.398	54.3	10.37	[2]
RA57	41.7	15.2	2.01	10.3	0.20	7.4	9.3	4.57	1.97	3.39	0.83	96.9	56.2	4.64	1.309	40.0	7.57	[6]
RPA02	44.0	11.7	2.03	10.4	0.16	13.1	10.0	2.46	1.07	3.58	0.59	99.0	69.3	3.18	0.814	35.3	7.13	[1]
RPA14	43.9	12.2	1.90	9.7	0.16	11.6	10.0	2.41	1.18	3.37	0.71	97.1	68.1	3.64	1.134	40.5	8.05	[2]
RPA21	44.3	12.9	1.90	9.7	0.15	10.3	10.6	2.63	1.21	3.62	0.72	98.0	65.5	3.80	1.064	42.6	8.33	[4]
RPA31	44.1	11.0	1.91	9.7	0.15	14.7	10.2	1.85	0.87	2.88	0.48	97.9	72.8	2.58	0.685	28.8	5.82	[2]
RPA71	44.2	11.8	1.95	10.0	0.16	12.7	9.5	2.06	1.10	3.22	0.62	97.2	69.4	3.23	0.870	35.7	7.10	[2]
Marotiri																		
MRT002	43.0	16.2	1.81	9.2	0.16	4.9	10.0	3.50	1.60	3.68	0.86	94.9	48.6	5.49	1.596	44.7	8.50	[7]
MRT003	45.5	16.7	1.70	8.7	0.16	3.6	8.7	2.93	2.20	3.16	1.00	94.3	42.6	6.68	1.367	58.0	11.09	[5]
MRT004	42.6	10.4	1.91	9.7	0.16	16.2	10.6	1.82	0.81	2.56	0.55	97.2	74.8	2.79	0.649	27.8	5.96	[2]
MRT006	46.3	17.1	1.72	8.7	0.16	3.6	8.4	3.02	2.10	3.20	1.01	95.3	42.0	6.54	1.701	62.3	11.99	[4]
MRT203	41.5	10.1	1.89	9.7	0.18	12.9	12.4	2.25	0.75	3.06	1.25	95.9	70.4	2.86	2.136	31.5	6.36	[2]
MRT204	37.5	9.6	1.90	9.7	0.16	14.8	13.1	1.67	0.52	2.96	1.43	93.2	73.1	2.55	1.497	28.1	5.70	[3]
Atiu																		
ATU104	45.9	15.3	1.76	9.0	0.20	5.1	10.2	3.17	1.28	3.25	0.62	95.8	50.5	5.12	1.365	44.1	8.56	[1]
ATU113	45.5	15.6	1.71	8.7	0.18	5.2	11.0	3.32	1.53	3.10	0.63	96.4	51.4	5.67	1.428	39.9	7.74	[1]
ATU114	43.9	8.6	1.98	10.1	0.19	18.3	9.3	1.87	0.74	2.16	0.40	97.4	76.4	3.45	0.885	28.0	5.47	[1]
ATU115	45.2	15.1	1.89	9.6	0.18	5.3	10.7	3.30	1.50	3.17	0.60	96.5	49.4	6.12	1.606	48.1	9.12	[1]
ATU123	44.5	10.1	1.89	9.6	0.17	14.2	10.3	1.98	0.85	2.19	0.36	96.1	72.4	3.29	0.832	28.9	6.02	[1]
ATU128	44.9	10.4	1.89	9.6	0.17	15.1	9.3	2.41	0.90	2.35	0.37	97.4	73.6	3.46	0.883	28.1	5.52	[1]
ATU132	45.0	14.5	1.85	9.4	0.18	6.1	11.2	3.20	1.34	2.89	0.56	96.2	53.6	6.14	1.510	44.2	8.29	[1]
ATU133	43.9	9.5	2.13	10.9	0.20	16.0	10.5	2.04	0.70	2.15	0.37	98.3	72.5	3.35	0.870	29.9	6.02	[1]
Rarotonga																		
RTG103	42.9	9.5	1.88	9.6	0.16	14.2	12.4	1.56	1.11	2.98	0.38	96.7	72.6	4.06	0.967	35.3	7.16	[3]
RTG104	44.8	9.2	1.80	9.2	0.17	15.2	11.6	1.05	1.04	2.37	0.34	96.7	74.6	3.59	0.785	30.8	6.40	[4]
RTG107	43.2	13.4	2.17	11.0	0.20	7.9	11.0	3.87	0.65	3.96	0.84	98.2	56.1	9.68	1.842	59.5	10.76	[4]
RTG110	44.4	14.4	1.96	10.0	0.17	6.4	10.8	2.59	2.00	3.44	0.58	96.7	53.1	6.08	1.428	47.4	9.12	[3]
RTG114	45.4	11.7	2.24	11.4	0.17	11.6	11.4	1.61	0.91	3.44	0.34	100.2	64.4	2.44	0.522	28.7	6.28	[4]
RTG115	44.1	9.0	1.96	10.0	0.17	15.4	12.1	1.46	0.89	2.55	0.34	98.0	73.3	3.72	1.088	32.5	6.57	[3]
RTG132	43.8	11.1	2.02	10.3	0.18	12.2	10.9	1.78	1.46	2.90	0.44	97.1	67.9	4.11	1.014	38.0	7.73	[3]
RTG141	44.6	12.7	1.97	10.1	0.18	8.4	11.6	2.47	1.82	3.24	0.56	97.4	59.7	5.83	1.378	44.2	8.92	[3]
RTG147	43.4	10.0	1.95	10.0	0.16	12.8	12.7	1.11	1.16	3.18	0.35	96.7	69.5	3.14	0.734	33.7	7.04	[3]
RTG161	44.1	12.1	1.90	9.7	0.18	9.7	11.2	2.62	1.73	3.14	0.56	97.0	64.0	6.22	1.373	45.2	8.60	[3]



Table 1. (continued)

Sample	SiO ²	Al ₂ O ₃	Fe ₂ O ₃	FeO	MnO	MgO	CaO	Na ₂ O	K ₂ O	TiO ₂	P ₂ O ₅	Total	Mg#	Th	U	Nd	Sm	Refs
Rururtu																		
RRT45	44.0	14.5	2.38	12.1	0.24	4.8	8.0	3.94	1.40	3.36	1.32	96.0	41.1	7.78	1.821	83.8	14.81	[3]
RRT60	45.9	14.8	2.22	11.3	0.20	5.5	7.3	4.37	1.35	3.40	0.91	97.3	46.5	6.16	1.659	61.5	11.40	[1]
RRT13	43.6	14.4	2.21	11.2	0.20	7.0	8.8	4.33	1.30	3.31	1.20	97.5	52.7	5.81	1.597	68.8	13.24	[2]
RRT10	43.5	14.2	2.27	11.5	0.22	6.7	8.7	4.59	1.42	3.27	1.22	97.7	50.8	5.67	1.537	66.3	12.58	[3]
RRT15	42.0	14.6	2.39	12.2	0.19	6.9	8.3	4.53	1.55	4.10	0.83	97.6	50.4	5.31	1.486	58.0	11.04	[1]
RRT56	41.4	14.6	2.44	12.4	0.20	7.3	8.5	4.23	1.56	4.47	0.86	97.9	51.1	5.09	1.433	55.9	11.20	[3]
RRT112B	47.4	15.1	1.36	6.9	0.11	3.9	11.5	3.03	0.87	3.89	0.70	94.7	50.0	4.45	1.528	50.3	10.28	[3]
RRT130	43.7	10.2	2.04	10.4	0.18	12.4	12.0	1.70	0.60	2.74	0.42	96.4	68.0	3.13	0.912	33.3	6.79	[2]
McDonald seamount																		
MCD110	42.8	13.4	2.06	10.5	0.17	9.8	10.4	3.54	1.36	3.84	0.69	98.5	62.6	4.96	1.348	48.7	9.37	[2]
MCD117	42.8	11.3	2.13	10.9	0.17	12.9	11.5	2.56	0.94	3.52	0.42	99.1	68.0	3.32	0.918	34.6	7.08	[3]
MCD206	41.4	15.2	1.99	10.2	0.17	6.5	10.3	3.76	1.05	4.34	0.60	95.4	53.2	4.63	1.055	45.3	9.06	[3]
MCD72	42.8	11.3	2.07	10.5	0.17	12.1	11.2	2.85	0.97	3.46	0.54	97.9	67.1	3.48	1.012	36.9	7.31	[1]
MCD79	42.4	10.3	2.09	10.7	0.17	14.9	10.7	2.47	0.93	3.50	0.42	98.5	71.3	2.96	0.859	34.1	7.14	[3]

References that provided the major element data presented here: [1] Dupuy et al. [1989]; [2] Dupuy et al. [1988]; [3] data original to this study collected at the Max-Planck-Institut für Chemie, Uni Mainz; [4] Kalfoun [2001]; [5] Liotard et al. [1990]; [6] Maury et al. [1978]; [7] Liotard and Barszcz [1985].

published works, and by extension single analytical methods, are presented here in an attempt to minimize interlaboratory biases; the data and their respective references are provided in the supporting information. Of particular relevance to the cumulative data set compiled here are the abundances of K, U, and Th, as these three elements are primarily responsible for the planet's radiogenic heat budget. Thorium abundances in each local suite of OIB, including the individual volcanic centers that constitute the Austral-Cook ocean island chain, are negatively correlated with MgO (Figures 2 and 3). The systematic variations in Th concentrations as a function of MgO likely represent the effects of variable degrees of fractional crystallization and/or olivine accumulation of the near-primary parental melt, although the role of different degrees of partial melting from the same (albeit heterogeneous) source cannot be discounted.

3.1. Cook-Austral Islands

[15] Bivariate linear regression trend lines (i.e., those that take into account uncertainties in both the *x* and *y* axes) plotting Th versus MgO abundances for lavas derived from the different volcanic centers in the Austral-Cook island chain, regardless of the age of eruption, have similar slopes and span a narrow range in *y* intercepts, indicating the progressive crystallization of a similar assemblage of minerals during the genesis of these rocks. Accordingly, samples with low MgO contents likely represent melts that have experienced subtraction of olivine ± clinopyroxene (± oxide) relative to the parental melt, whereas samples with high MgO contents have accumulated

early-crystallizing phases, similar to the olivine subtraction/ addition trends identified in Hawaiian

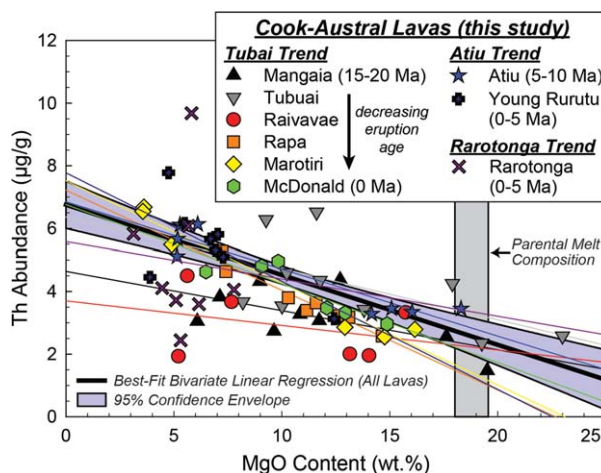


Figure 2. Thorium abundances (in µg/g) and MgO contents (in wt %) of the Cook-Austral lavas analyzed here. Thorium represents the most highly incompatible element that is neither fluid-mobile nor sensitive to redox conditions, and MgO acts as a proxy to fractional crystallization. Whether considering each volcanic center individually or evaluating the Cook-Austral data set as a whole, negative trends between Th and MgO are preserved and show similar bivariate linear regression statistics (Table 4). The age of each volcanic center has no significant influence on the regression statistics. Bivariate linear regression trend lines are provided for each volcanic center and follow the same color scheme provided in the key. Statistical scatter observed in low-MgO samples (particularly Rarotonga lavas) may represent: (1) contamination and/or assimilation of small quantities of pelagic sediment; (2) late crystallization of a phase in which Th is compatible; or (3) instability of a Th-rich phase at low MgO. [Color figure can be viewed in the online issue, which is available at wileyonlinelibrary.com.]

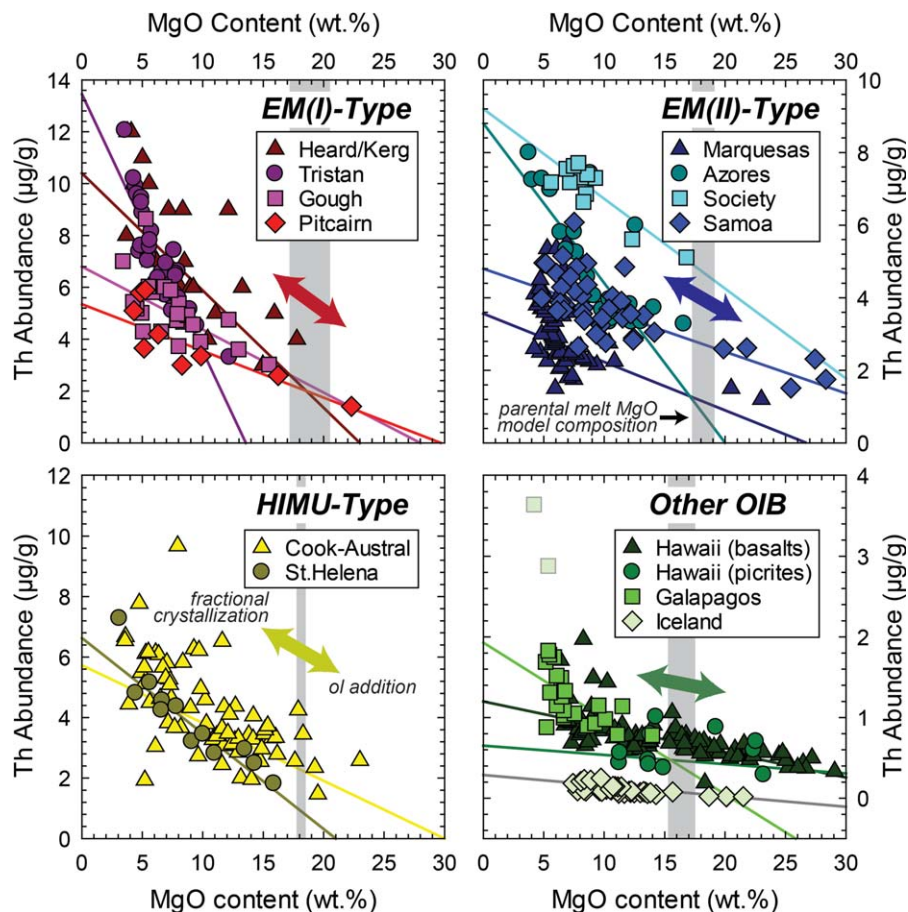


Figure 3. Thorium abundances (in $\mu\text{g/g}$) and MgO contents (in wt %) of the new and published OIB data compiled in this study. All OIB localities show negative correlations between Th and MgO, following the trend observed in Cook-Austral lavas (Figure 2). Samples with lower MgO contents than their respective parental melts likely represent lavas that have experienced subtraction of olivine \pm clinopyroxene (\pm oxide), whereas samples with higher MgO contents have accumulated early-crystallizing phases. Note the different scales on the ordinate axis of each plot; samples derived from Hawaii, Galapagos, and Iceland exhibit significantly lower Th abundances than HIMU- and EM-type lavas. The bivariate linear regression statistics for each OIB suite are provided in Table 4. The sources for the published data plotted above are as follows: Heard/Kerguelen [Barling et al., 1994]; Tristan da Cunha and Gough [Willbold and Stracke, 2006]; Pitcairn [Caroff et al., 1993]; Marquesas [Caroff et al., 1999]; Azores [Beier et al., 2007]; Society [Hemond et al., 1994]; Samoa [Workman et al., 2004]; Hawaii (basalts; Huang and Frey [2003], EPSL; picrites: Ireland et al. [2009]); Galapagos [Geist et al., 2003]; Iceland [Stracke et al., 2003]; and St. Helena [Willbold and Stracke, 2006]. These data can be downloaded from the supporting information. [Color figure can be viewed in the online issue, which is available at wileyonlinelibrary.com.]

picrites [e.g., Ireland et al., 2009]. In order to determine the composition of the parental melts more precisely from each volcanic center, we do not attempt to determine the exact fractionation path for each volcanic center, but rather correct the composition of each individual lava with 7.5–16 wt % MgO from each volcanic center to bring them into equilibrium with olivine of Fo90, assuming $(\text{Fe}^{2+}/\text{Mg})_{\text{ol}}/(\text{Fe}^{2+}/\text{Mg})_{\text{wr}} = 0.3$ [e.g., Roeder and Emslie, 1970; Putirka, 2005] and $\text{Fe}^{2+}/\text{Fe}_{\text{total}} = 0.88$ [e.g., Bezos and Humler, 2005;

Rhodes and Vollinger, 2005]. Similar to the method employed by Dasgupta et al. [2010], we add stoichiometrically pure olivine [i.e., $(\text{Fe},\text{Mg})_2\text{SiO}_4$] and clinopyroxene with a fixed composition (i.e., representative of intraplate alkali basalts) [Nisbet and Pierce, 1977] in constant (but not necessarily equal) proportions in order to reproduce the slope of the $\text{CaO}/\text{Al}_2\text{O}_3$ versus MgO plot for each volcanic center (see supporting information). Of note, the parental melt compositions derived from each volcanic center and the average parental



Table 2. Near-Primary Melt Model Compositions^{a,b} (in wt %) for Different Volcanic Centers in the Cook-Austral Ocean Island Chain

Volcanic Center	SiO ₂	TiO ₂	Al ₂ O ₃	FeO	MnO	MgO	CaO	Na ₂ O	K ₂ O	P ₂ O ₅	Total	n
Mangaia ± 2σ _m	43.9 ± 0.3	1.92 ± 0.10	7.67 ± 0.28	11.2 ± 0.4	0.184 ± 0.006	18.8 ± 0.7	11.1 ± 0.9	1.58 ± 0.27	0.415 ± 0.050	0.276 ± 0.024	97.1 ± 1.3	6
Tubuai ± 2σ _m	43.6 ± 0.7	1.86 ± 0.10	7.55 ± 0.39	11.8 ± 0.7	0.193 ± 0.012	19.9 ± 1.1	9.73 ± 1.27	1.60 ± 0.60	0.450 ± 0.135	0.295 ± 0.094	97.0 ± 2.1	7
Raiavae ± 2σ _m	46.0 ± 1.0	1.87 ± 0.08	9.32 ± 0.68	10.5 ± 0.4	0.154 ± 0.011	17.7 ± 0.6	8.99 ± 0.90	1.98 ± 0.12	0.491 ± 0.093	0.279 ± 0.037	97.3 ± 1.7	4
Rapa ± 2σ _m	44.2 ± 0.3	2.68 ± 0.08	9.41 ± 0.21	10.5 ± 0.2	0.157 ± 0.003	17.7 ± 0.3	9.32 ± 0.40	1.81 ± 0.10	0.815 ± 0.031	0.483 ± 0.036	97.0 ± 0.7	6
Marotiri ± 2σ _m	40.9 ± 2.8	2.59 ± 0.13	9.05 ± 0.98	10.1 ± 0.1	0.164 ± 0.011	17.1 ± 0.1	11.4 ± 1.2	1.73 ± 0.21	0.616 ± 0.182	0.937 ± 0.437	94.6 ± 3.2	3
Aitu ± 2σ _m	44.3 ± 0.6	2.04 ± 0.16	8.98 ± 0.73	10.4 ± 0.8	0.175 ± 0.016	17.6 ± 1.3	9.62 ± 0.55	1.94 ± 0.30	0.724 ± 0.126	0.324 ± 0.015	96.1 ± 1.9	3
Rarotonga ± 2σ _m	44.0 ± 0.4	2.36 ± 0.12	8.14 ± 0.32	10.8 ± 0.5	0.171 ± 0.007	18.2 ± 0.9	10.7 ± 0.6	1.42 ± 0.25	0.857 ± 0.175	0.314 ± 0.034	96.9 ± 1.4	9
Rurutu ± 2σ _m	43.6 ± N/A	2.17 ± N/A	7.85 ± N/A	10.9 ± N/A	0.173 ± N/A	18.4 ± N/A	10.7 ± N/A	1.35 ± N/A	0.438 ± N/A	0.307 ± N/A	96.1 ± N/A	1
Macdonald ± 2σ _m	43.1 ± 0.3	2.69 ± 0.16	8.52 ± 0.16	11.3 ± 0.2	0.168 ± 0.004	19.0 ± 0.3	9.9 ± 0.3	2.14 ± 0.11	0.747 ± 0.057	0.355 ± 0.036	97.8 ± 0.6	5
Average	43.7 ± 1.3	2.24 ± 0.01	8.50 ± 0.29	10.8 ± 0.2	0.171 ± 0.000	18.3 ± 0.6	10.2 ± 0.7	1.73 ± 0.08	0.617 ± 0.014	0.397 ± 0.026	96.6 ± 1.6	44
Cook-Austral^c ± 2σ_m	43.8 ± 0.4	2.25 ± 0.11	8.42 ± 0.25	10.9 ± 0.2	0.172 ± 0.005	18.4 ± 0.4	10.1 ± 0.4	1.71 ± 0.13	0.646 ± 0.069	0.373 ± 0.059	96.9 ± 0.8	44
Composite												
Cook-Austral^d ± 2σ_m												

^aOnly lavas with 7.5 wt % ≤ MgO content ≤ 16 wt % were considered for these calculations.

^bOlivine (i.e., trace-element free (Mg,Fe)₂SiO₄) and clinopyroxene (i.e., average composition measured in intraplate alkali basalts; Nisbet and Pierce [1977]) were added in order to reconstruct CaO/Al₂O₃ versus MgO trends and force equilibrium with Fo90 olivine.

^cStatistical average of the individual Cook-Austral ocean islands reported in this table.

^dIndependent linear regression of inclusive Cook-Austral data set.

melt composition of all Austral-Cook lavas considered collectively give statistically indistinguishable results (Table 2).

[16] The parental melt composition derived from the Cook-Austral source contains 18.4 ± 0.4 ($2\sigma_m$) wt % MgO (Tables 2 and 3), which is in agreement with the average “reference” near-primary composition of the Cook-Austral islands (18.6 ± 1.1 wt % MgO) proposed by Dasgupta et al. [2010] based on an independent evaluation of a compiled data set (Figure 4). According to Th versus MgO bivariate linear regression statistics provided in Table 4, we conclude that the parental melt from the Cook-Austral source contains 2.2 ± 0.2 ($2\sigma_m$; $n=9$ volcanic centers) μg/g Th, which is approximately 10 times more concentrated than the composition of global MORB (i.e., approximately 0.24 μg/g Th) [Arevalo and McDonough, 2010; Jenner and O’Neill, 2012; Gale et al., 2013; White and Klein, 2013].

3.2. Other HIMU- and EM-Type OIB

[17] In addition to the lavas from the Cook-Austral Islands, negatively correlated linear trends between highly incompatible Th and MgO abundances are observed in OIB derived from HIMU-type St. Helena; EM(I)-type Heard, Tristan da Cunha, Gough, and Pitcairn; and EM(II)-type Marquesas, Azores, Society, and Samoa (Figure 3). Lavas from other OIB localities, such as Hawaii, Galapagos, and Iceland, also show negative linear correlations between Th and MgO, albeit with shallower slopes than samples derived from localities that define the isotopic end-members in Figure 1. Further, these non-end-member lavas are significantly less enriched in Th compared to samples from HIMU- and EM-type volcanic chains, which are comparably enriched in Th in primitive lavas with 15–20 wt % MgO. This discrepancy in the absolute abundances of Th in lavas derived from Hawaii, Galapagos, and Iceland compared with those from end-member-type localities may reflect either (1) gross differences in degrees of melting; (2) distinct source lithologies (i.e., peridotite versus pyroxenite, which are discussed below); (3) incorporation of a mantle component with a distinct but non-end-member isotopic signature (i.e., the Focal Zone, “FOZO,” or Common Component, “C”) [e.g., Hart, 1988; Hanan and Graham, 1996; Stracke et al., 2005]; (4) a greater fraction of depleted upper mantle materials that have been entrained/assimilated during ascent and emplacement of



Table 3. Near-Primary Melt Model Compositions^{a,b} (in wt %) for Various End-Member OIB Localities

OIB Locality	SiO ₂	TiO ₂	Al ₂ O ₃	FeO	MnO	MgO	CaO	Na ₂ O	K ₂ O	P ₂ O ₅	Total	Reference
<i>Hybrid-Type</i>												
Hawaii (lavas) ± 2σ _m	47.1 ± 0.4	1.96 ± 0.05	9.90 ± 0.09	10.5 ± 0.2	0.151 ± 0.004	17.6 ± 0.3	8.48 ± 0.15	1.55 ± 0.04	0.239 ± 0.026	0.197 ± 0.009	97.6 ± 0.5	Huang and Frey [2003]
Hawaii (picrites) ± 2σ _m	48.9 ± 0.2	1.69 ± 0.11	10.4 ± 0.1	9.83 ± 0.09	0.157 ± 0.006	16.6 ± 0.2	8.41 ± 0.06	1.60 ± 0.06	0.276 ± 0.038	0.158 ± 0.008	98.0 ± 0.3	Ireland et al. [2009]
Galapagos ± 2σ _m	47.1 ± 0.3	1.91 ± 0.09	13.08 ± 0.58	9.00 ± 0.36	0.123 ± 0.025	15.2 ± 0.6	10.0 ± 0.4	2.02 ± 0.08	0.339 ± 0.025	0.193 ± 0.016	99.0 ± 1.0	Geist et al. [2006]
Iceland ± 2σ _m	47.7 ± 0.2	0.749 ± 0.066	13.19 ± 0.36	8.95 ± 0.30	0.160 ± 0.003	15.1 ± 0.5	11.4 ± 0.3	1.53 ± 0.02	0.054 ± 0.007	0.039 ± 0.008	98.8 ± 0.8	Siracke et al. [2003]
<i>EMII-Type</i>												
Heard Island ± 2σ _m	45.8 ± 1.0	2.78 ± 0.34	7.81 ± 0.46	11.0 ± 0.3	0.163 ± 0.008	18.5 ± 0.6	8.98 ± 0.35	1.91 ± 0.15	1.46 ± 0.15	0.414 ± 0.061	98.8 ± 1.4	Barling et al. [1994]
Tristan da Cunha ± 2σ _m	43.7 ± 0.8	2.11 ± 0.08	6.24 ± 0.35	12.1 ± 0.5	0.202 ± 0.013	20.4 ± 0.9	11.7 ± 0.2	1.21 ± 0.23	0.537 ± 0.156	0.215 ± 0.134	98.4 ± 1.4	Willbold and Siracke [2006]
Gough Island ^b ± 2σ _m	46.2 ± 0.4	2.42 ± 0.08	9.72 ± 0.20	10.15 ± 0.23	0.134 ± 0.005	17.1 ± 0.4	7.34 ± 0.17	1.98 ± 0.11	1.53 ± 0.13	0.449 ± 0.048	97.0 ± 0.7	Willbold and Siracke [2006]
Pitcairn ± 2σ _m	43.0 ± 1.0	2.85 ± 0.11	8.15 ± 0.56	11.5 ± 0.5	0.158 ± 0.004	19.5 ± 0.9	9.18 ± 0.48	1.48 ± 0.01	0.456 ± 0.091	0.340 ± 0.019	96.6 ± 1.7	Caroff et al. [1993]
<i>EMII-Type</i>												
Marquesas ± 2σ _m	45.2 ± 0.4	2.29 ± 0.08	9.44 ± 0.17	11.3 ± 0.2	0.139 ± 0.003	19.0 ± 0.4	7.61 ± 0.29	1.86 ± 0.09	0.543 ± 0.122	0.287 ± 0.028	97.6 ± 0.7	Caroff et al. [1999]
Azores ± 2σ _m	45.3 ± 0.4	2.41 ± 0.09	9.07 ± 0.37	10.14 ± 0.32	0.174 ± 0.004	17.1 ± 0.5	10.3 ± 0.3	1.82 ± 0.12	0.97 ± 0.10	0.352 ± 0.024	97.6 ± 0.9	Beier et al. [2007]
Society Islands ± 2σ _m	44.2 ± 0.3	2.63 ± 0.06	9.04 ± 0.10	11.3 ± 0.1	0.145 ± 0.010	19.0 ± 0.1	8.14 ± 0.24	1.99 ± 0.04	1.22 ± 0.05	0.433 ± 0.018	98.1 ± 0.4	Hemond et al. [1994]
Samoa ± 2σ _m	45.9 ± 0.3	2.37 ± 0.12	9.35 ± 0.22	10.6 ± 0.3	0.153 ± 0.003	17.9 ± 0.5	9.9 ± 0.4	1.81 ± 0.04	0.708 ± 0.050	0.263 ± 0.014	99.0 ± 0.8	Workman et al. [2003]
<i>HIMU-Type</i>												
St. Helena ± 2σ _m	44.1 ± 0.3	1.94 ± 0.05	8.92 ± 0.44	10.6 ± 0.4	0.180 ± 0.007	17.9 ± 0.7	10.7 ± 0.7	1.45 ± 0.12	0.518 ± 0.044	0.264 ± 0.022	96.6 ± 1.2	Willbold and Siracke [2006]
Composite	43.8 ± 0.4	2.25 ± 0.11	8.42 ± 0.25	10.9 ± 0.2	0.172 ± 0.005	18.4 ± 0.4	10.1 ± 0.4	1.71 ± 0.13	0.646 ± 0.069	0.373 ± 0.059	96.9 ± 0.8	This study
Cook-Austral ± 2σ _m												

^aOnly lavas with 7.5 wt % ≤ MgO content ≤ 16 wt % were considered for these calculations.

^bOlivine (i.e., trace-element free (Mg,Fe)₂SiO₄) and clinopyroxene (i.e., average composition measured in ocean floor basalts; Nisbet and Pierce [1977]) were added to reconstruct CaO/Al₂O₃ versus MgO trends and force equilibrium with Fo90 olivine.

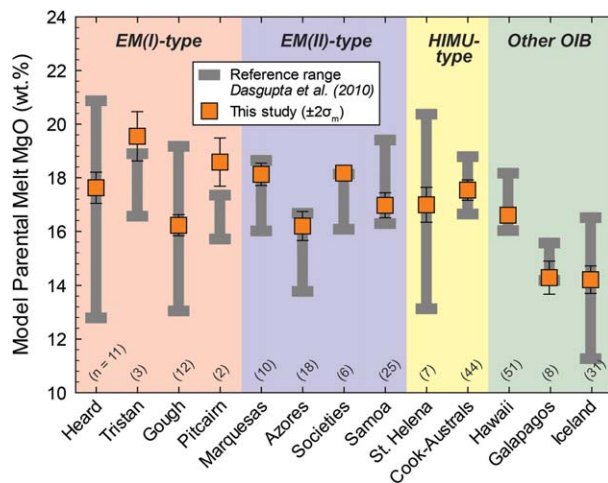


Figure 4. Comparison of the MgO contents of the parental melt compositions determined here versus those estimated by Dasgupta et al. [2010] for sample suites derived from HIMU-, EM(I)-, and EM(II)-type localities, as well as Hawaii, Galapagos, and Iceland. The uncertainties reported by Dasgupta et al. [2010] represent 2σ statistical deviations measured in independent collections of samples from the same OIB localities as those investigated here. In this study, we report $2\sigma_m$ deviations by assuming the composition of each individual lava with 7.5–16 wt % MgO from each volcanic center to bring them into equilibrium with olivine of Fo90, assuming $(\text{Fe}^{2+}/\text{Mg})_{\text{ol}}/(\text{Fe}^{2+}/\text{Mg})_{\text{wr}} = 0.3$ and $\text{Fe}^{2+}/\text{Fe}_{\text{total}} = 0.88$ (see text for discussion); the numbers of lavas with 7.5–16 wt % MgO from each OIB locality are given in parentheses. [Color figure can be viewed in the online issue, which is available at wileyonlinelibrary.com.]

Hawaii, Galapagos, and Iceland lavas; or (5) some combination of these. The distinct slope for each Th versus MgO trend line, regardless of absolute enrichment, indicates the fractionation of different proportions and/or compositions of early-crystallizing phases (namely, olivine \pm clinopyroxene \pm oxide).

[18] For the purpose of our model, we have determined the parental melt composition from the lavas from each hotspot locality considered here (Table 3). Without exception, the parental melts from each end-member-type locality (i.e., HIMU and EM sources) center around 17–19 wt % MgO. Conversely, lavas from Hawaii, Iceland, and Galapagos have parental melt compositions between 15 and 17 wt % MgO, similar to previous studies of near-primary melts derived from Hawaii [Norman and Garcia, 1999; Ireland et al., 2009]. A comparison of the MgO contents of our model parental melt compositions relative to the “reference” near-primary compositions determined by Dasgupta et al. [2010] is provided in Figure 4.

[19] The best fit linear regression of Th versus MgO for the Tristan da Cunha lavas indicates that either the crystallizing assemblage of minerals in these samples changed (i.e., a cotectic point was reached) as the lavas approached ~ 10 wt % MgO, or the parental melt of these samples must have had a lower MgO content (i.e., ≤ 14 wt %) than the lavas from the other localities considered here; the lack of high MgO samples from Tristan da Cunha (only one sample with > 10 wt % MgO) makes extrapolation to the parental melt composition tenuous, and therefore, this locality is not considered in the OIB source model presented here.

[20] Using the bivariate linear regression statistics provided in Table 4, we infer the abundances of Th in the parental melts of the various OIB localities explored here. The results of these calculations, which are also provided in Table 4, serve to illustrate that the parental melts of all end-member-type localities share similar enrichments in Th. All near-primary melt model compositions derived from the end-member-type localities considered here, with the exception of Tristan da Cunha which is discussed above, contain 1.0–4.4 $\mu\text{g/g}$ Th, with an average composition of 2.1 ± 0.3 ($2\sigma_m$; $n = 9$ localities) $\mu\text{g/g}$ Th. Alternatively, the near-primary model compositions of lavas derived from Hawaii, Galapagos, and Iceland contain only 0.04–0.62 $\mu\text{g/g}$ Th, with an average composition of 0.39 ± 0.16 ($2\sigma_m$; $n = 4$) $\mu\text{g/g}$ Th that is more than five times lower than the mean composition of the end-member-type parental melts.

4. Determining OIB Source Compositions Via Inverse Modeling

[21] We can estimate the incompatible element budget of the Cook-Austral source region, as well as the sources of the other OIB localities considered here, by inverse modeling following a simplified model of partial melting. Generally, MORB are thought to form by large degrees of melting (i.e., $F \approx 8$ –15%) [e.g., Klein and Langmuir, 1987; McKenzie and Bickle, 1988; Niu, 1997; Salters and Stracke, 2004]. In comparison, intra-plate alkali basalts, such as the OIB samples analyzed here, reflect lower degrees of partial melting, as inferred from elevated incompatible element abundances [e.g., Hofmann, 1988; Sun and McDonough, 1989], silica undersaturation [e.g., Green and Ringwood, 1967; Gast, 1968; Green, 1970], and trace element fractionations



Table 4. Linear Regression ($y = mx + b$) Statistics of Trends Between Th and MgO Contents of OIB Lavas and Near-Primary Melt and Source Model Calculations

Ocean Island Locality	Slope (m)	95% Confidence Interval	Intercept (b)	95% Confidence Interval	y	95% Confidence Interval	n	Near-Primary MgO (wt%)	2 σ	2 σ_m	Near-Primary Th ($\mu\text{g/g}$)	95% Confidence Interval	Source Th (ng/g) ^a	95% Confidence Interval	2 σ_m	T Value ^b ($\alpha = 0.01$)	T_{critical}	
<i>HIMU-Type</i>																		
Mangaia	-0.15	0.10	4.70	1.30	10	18.8	1.8	0.7	1.9	2.3	140	170	140	50	0.4	3.2		
Tubuai	-0.15	0.14	5.90	2.20	10	19.9	2.9	1.1	2.9	3.6	220	280	220	90	0.7	3.2		
Raiavavae	-0.02	0.25	2.60	2.90	6	17.7	1.2	0.6	2.2	5.3	170	400	170	160	0.1	3.7		
Rapa	-0.31	0.05	7.15	0.55	8	17.7	0.8	0.3	1.6	1.0	120	90	120	30	1.1	3.4		
Marotiri	-0.33	0.11	7.50	1.30	5	17.1	0.2	0.1	1.9	2.3	140	180	140	80	0.3	4.0		
Atiu	-0.21	0.08	6.80	1.10	8	17.6	2.2	1.3	3.1	1.9	230	160	230	60	1.2	3.4		
Rarotonga	-0.66	0.46	12.00	5.10	10	18.2	2.8	0.9	0.0	10.0	0	0	0	0	8.5	3.2		
Rurutu	-0.30	0.30	7.20	2.40	8	18.4	1.6	0.7	1.7	6.0	130	470	130	170	0.2	3.4		
Macdonald	-0.26	0.17	6.80	2.00	5	19.0	0.6	0.3	1.9	3.8	140	290	140	130	0.2	4.0		
Average Cook-Austral ^c	-0.27	0.07	6.74	0.82	70	18.3	0.6	0.3	1.9	1.6	140	130	140	20	0.6	2.7		
Composite Cook-Austral ^d	-0.19	0.07	5.68	0.80	70	18.4	2.5	0.4	2.2	1.5	160	120	160	10	0.0	2.7		
St. Helena	-0.32	0.10	6.70	0.97	12	17.9	1.7	0.7	1.0	2.1	70	150	70	40	1.9	3.1		
<i>Enriched Mantle-Type EM(I)-Type</i>																		
Heard Island	-0.47	0.20	10.80	2.00	22	18.5	1.9	0.6	2.1	4.3	160	330	160	70	0.0	2.8		
Tristan da Cunha ^e	-1.01	0.23	13.60	1.50	31	20.4	1.6	0.9	N/A	N/A	N/A	N/A	N/A	N/A	N/A	N/A		
Gough Island	-0.24	0.12	6.70	1.00	23	17.1	1.4	0.4	2.6	2.3	190	180	190	40	0.6	2.8		
Pitcairn	-0.18	0.10	5.30	1.20	9	19.5	1.3	0.9	1.8	2.2	140	180	140	60	0.3	3.3		
<i>EM(II)-Type</i>																		
Marquesas	-0.14	0.07	3.60	0.55	59	19.0	1.3	0.4	1.0	1.5	80	120	80	20	2.6	2.7		
Azores	-0.44	0.15	8.80	1.50	25	17.1	2.3	0.5	1.3	3.1	100	250	100	50	0.9	2.8		
Society Islands	-0.25	0.08	9.10	0.80	12	19.0	0.3	0.1	4.4	1.7	330	170	330	50	3.1	3.1		
Samoa	-0.11	0.03	4.74	0.39	42	17.9	2.3	0.5	2.7	0.7	210	90	210	10	2.0	2.7		
Average End-Member-Type OIB									2.1	0.8	160	60	160	20	N/A	N/A		
<i>Other OIB</i>																		
Hawaii (lavas)	-0.033	0.005	1.20	0.09	98	17.6	2.0	0.3	0.62	0.13	47	19	47	2	17.2	2.6		
Hawaii (picrites)	-0.009	0.024	0.61	0.42	11	16.6	0.4	0.2	0.46	0.58	35	45	35	14	5.6	3.1		
Galapagos	-0.098	0.068	1.91	0.54	25	15.2	1.7	0.6	0.42	1.17	32	89	32	18	4.9	2.8		
Iceland	-0.014	0.005	0.258	0.064	38	15.1	2.8	0.5	0.04	0.10	3	7	3	1	19.4	2.7		

^aSource composition modeled assuming $7.5 \pm 2.5\%$ modal fractional melting of a dominantly peridotitic source.

^b T value from independent two-sample t test of two distributions with different sample sizes but equal variance; T value $< T_{\text{critical}}$ indicates the two distributions are statistically indistinguishable.

^cStatistical average of the individual Cook-Austral ocean islands reported in this table.

^dIndependent linear regression of inclusive Cook-Austral data set.

^eThe incompatible element abundances in the Tristan lavas examined here cannot be reconciled to a parental melt with ≥ 14 wt % MgO.



[e.g., *Sims et al.*, 1995]. Both MORB and OIB trace element compositions can be approximated by dynamic, near-fractional melting [e.g., *Langmuir et al.*, 1977; *Johnson et al.*, 1990; *Spiegelman and Kenyon*, 1992]; consequently, we adapt a simplified model of accumulated fractional melting [*Shaw*, 1970], whereby the composition of the OSRs with respect to element i (i.e., C_i^{OSR}) may be defined by only three variables (assuming modal melting): the composition of the near-primary parental melt with respect to element i (C_i^{OIB}); the partition coefficient of element i between the solid and liquid ($D_i^{\text{sol/liq}}$); and the fraction of melting (F), according to the relationship:

$$C_i^{\text{OSR}} = \frac{C_i^{\text{OIB}} \times F}{1 - (1 - F)^{1/D_i^{\text{sol/liq}}}}. \quad (2)$$

[22] This oversimplification allows us to estimate the source composition by defining only one intensive property (i.e., $D_i^{\text{sol/liq}}$), one extensive property (C_i^{OIB}), and a single unknown variable (F). However, a number of fundamental assumptions are required for the inversion calculations employed here to apply to OIB source melting:

- (1) Melting occurs as imperfect fractional melting of an invariant proportion of minerals constituting the source lithology, thereby allowing for the application of modal accumulated partial melting equations [*Shaw*, 1970];
- (2) The bulk partition coefficients of the elements involved (i.e., $D_{\text{Th}}^{\text{sol/liq}}$) are constant and well constrained during melting;
- (3) Lavas from each OIB locality are cogenetic (derived from a common source region);
- (4) The degree of heterogeneity of the investigated mantle sources is adequately reflected in the OIB sample suites analyzed here [*Stracke and Bourdon*, 2009].

[23] Further, because there is no well-defined method for estimating a representative or average degree of melting of an OSR without assuming a source lithology/composition, absolute abundance of trace elements in the mantle source, or constancy of source ratios of incompatible elements, we are forced to account for a range of F values.

[24] As mentioned earlier, the degrees of melting represented by alkali OIB are generally believed to be less than the 8–15% melting that produces tholeiitic MORB [*Klein and Langmuir*, 1987; *McKenzie and Bickle*, 1988, *Niu*, 1997]. Petrogenetic models of melting/crystallization relations [*Gast*, 1968; *Sun and Hanson*, 1975], composi-

tional variations observed in mantle peridotites [*Frey et al.*, 1978] and OIB [*Sims et al.*, 1999; *Putirka*, 2008], and anhydrous peridotite melting experiments [*Jaques and Green*, 1980] suggest that alkali basalts are derived from $\leq 10\%$ partial melting of their respective sources. This has been corroborated by multiple studies of Hawaiian alkali basalts, which have been estimated to reflect between 3 and 12% accumulated incremental melting according to: major element lava compositions and peridotite melting experiments [*Chen*, 1988]; trace element systematics in lavas [*Norman and Garcia*, 1999; *Feigenson et al.*, 2003; *Maaløe and Pedersen*, 2003] and olivine-hosted melt inclusions [*Norman et al.*, 2002]; dynamic melting models that incorporate phase-equilibria constraints and variable partition coefficients [*Eggins*, 1992]; and numerical modeling of the Hawaiian swell [*Watson and McKenzie*, 1991].

[25] We assume 5–10% melting of the OIB sources considered here based on the constraints listed above, as well as trace element modeling of Th/Nd and U/Sm systematics following the protocols established by *Treuil and Joron* [1975], *Minster and Allègre* [1978], and *Maaløe and Pederson* [2003]; these trace element models, which can be found in the supporting information, not only serve to illustrate the difficulty in establishing degrees of partial melting but also verify that our 5–10% melting model is consistent with trace element trends observed and extrapolated in the samples analyzed here. We then inversely model the composition of the source of each OIB locality based on the model parental melt compositions determined in Table 4 and a bulk partition coefficient of $D^{\text{sol/liq}}(\text{Th}) = 0.003 \pm 0.001$ ($2\sigma_m$) derived from experimental melting experiments of garnet peridotite between 1.0 and 3.4 GPa [*Salter and Longhi*, 1999; *Salter et al.*, 2002; *Salter and Stracke*, 2004].

[26] In order to consider the impact of a pyroxenitic source lithology, we can derive a bulk partition coefficient of $D^{\text{sol/liq}}(\text{Th}) = 0.005 \pm 0.002$ ($2\sigma_m$) based on melting experiments of MORB-like pyroxenite and eclogite at 2.9–3.1 GPa [*Klemme et al.*, 2002; *Pertermann et al.*, 2004] (see supporting information). This exercise yields a minor deviation from our baseline that trivially affects our inverse source model and corroborates other studies that have shown that the bulk partitioning behavior of Th (and U) does not vary significantly between peridotitic and pyroxenitic sources [e.g., *Stracke et al.*, 2006; *Prytulak and Elliott*, 2009; *Koornneef et al.*, 2012]. However,



pyroxenic source components have been shown to melt with a much higher production rate and at greater pressures/depths than ambient mantle peridotite [Yaxley, 2000; Hirschmann *et al.*, 2003; Pertermann and Hirschmann, 2003]. Thus, 5–10% partial melting of the OIB sources considered here may actually be an underestimation of the true degree of melting experienced by each volcanic center, should pyroxenitic components play a significant role in the source lithologies of our OIB sample suites. As a result, our baseline model may actually represent a lower bound on the enrichment of the investigated OIB sources.

5. Implications and Discussion

5.1. Minimum Enrichment of OIB Sources, as Observed in HIMU- and EM-Type Lavas

[27] Despite uncertainties in the exact mineralogy/petrology of the sources of the lavas analyzed here, our model constrains the relative enrichment of end-member-type OIB sources; this is accomplished by assuming a peridotitic source lithology and a suitable range of degrees of melting required to produce the near-primary parental melt compositions determined here. Moreover, the estimated OIB source concentrations derived here represent average source compositions; the degree of heterogeneity of the investigated OSR that is reflected in the lavas analyzed here is dependent on the effectiveness of melt mixing during melting and melt extraction as well as source and melting-induced compositional variability. Individual components in these heterogeneous OIB sources may be more or less enriched than the average composition estimated here. For example, if OIB lavas originate from mantle plumes that entrain significant amounts of depleted upper mantle materials upon ascent and emplacement, as has been suggested by experimental and numerical simulations [e.g., Griffiths and Campbell, 1990; Neavel and Johnson, 1991; van Keken, 1997; Davaille, 1999; Kumagai, 2002; Lin and van Keken, 2006], then our modeled average OIB source compositions certainly represents only a lower bound on the enrichment (and thus an upper limit on the volume) of this reservoir.

[28] According to the parental melt compositions modeled in Table 4 and following 5–10% accumulated fractional melting of the sources of these magmas, we estimate that the sources of these OIB end-member lavas contain between 70 and 330 ng/g Th,

with a mean composition of 160 ± 20 ($2\sigma_m$) ng/g Th. The average model composition of the HIMU- and EM-type OIB sources reconstructed here is coincidentally similar to that of global MORB, which are characterized by a representative composition of ~ 240 ng/g Th (Table 5). The BSE quantitatively comprises the CC and mantle and contains 79 ng/g Th according to traditional geochemical models (Table 6); therefore, the enrichment of Th in the OSR defined here is twice that of the BSE, implying a source with a significant amount of recycled oceanic crust [Hofmann and White, 1982].

[29] Conversely, the sources of the lavas from Hawaii, Iceland, and the Galapagos are modeled to contain between 3 and 47 ng/g Th, significantly more depleted in highly incompatible elements than the BSE and the sources of end-member-type OIB. In order to reconcile the compositions of the sources of Hawaii, Iceland, and the Galapagos with those of end-member-type OIB, the parental melts of the lavas analyzed here would need to represent $\geq 30\%$ partial melting in the case of Hawaii, $\geq 40\%$ for the Galapagos, and a numerically impossible solution (i.e., $F > 100\%$) for Iceland. Thus, this discrepancy in model compositions likely reflects melting of distinct source components and/or the entrainment of a larger fraction of depleted mantle materials.

5.2. Size and Radiogenic Heat Production of the OSR

[30] The degree of enrichment of the OSR(s) has important implications for mass balance and the chemical structure of the modern mantle as well as the radiogenic heat budget of the planet. Temporarily ignoring evidence for an enriched, early-formed, and/or unsampled mantle reservoir, as suggested by several geochemical studies [e.g., Rudnick *et al.*, 2000; Boyet and Carlson, 2005; Tolstikhin and Hofmann, 2005], we can simplify the modern mantle into two fundamental chemical units: the source of MORB (DMM); and a more enriched OSR. Regardless of the architecture of these two mantle components, whether they are preserved by a uniform or undulating thermochemical boundary layer [e.g., Kellogg *et al.*, 1999; van der Hilst and Káráson, 1999], or enriched blobs [e.g., Becker *et al.*, 1999] and/or streaks [e.g., Allègre and Turcotte, 1986; Morgan and Morgan, 1999] of OIB source material suspended in a matrix of DMM, mass balance (see equation (1)) dictates that the larger the mass of



Table 5. Model Compositions for the Depleted MORB Mantle (DMM) Based on Average Global MORB (G-MORB), Normal-Type MORB [N-MORB; e.g. (La/Sm)_N < 1], and Abyssal Peridotite Compositions^a

Element	G-MORB DMM Models ^b						N-MORB DMM Models ^c								
	A&McD10		J&O12		Getal13		W&K(p)		G-MORB DMM		N-MORB DMM		Peridotite DMM		
	Median	Log-normal mean	Median	Log-normal mean	Median	Log-normal mean	Median	Log-normal mean	Model ^e	Model ^e	Model ^d	Model ^d	Model ^e	Model ^e	
K ($\mu\text{g/g} \pm 2\sigma_m$)	100	150 \pm 30	110	110 \pm 10	110	120 \pm 10	90	90 \pm 20	110 \pm 10	88 \pm 16	60	60 \pm 17	100 \pm 20	77 \pm 33	50 \pm 8
Th (ng/g) $\pm 2\sigma_m$	17	22 \pm 3	22.8	24 \pm 3	25	29 \pm 3	23	27 \pm 2	24 \pm 1	19 \pm 5	12	14 \pm 4	14 \pm 2	15 \pm 7	7.9 \pm 1.1
U (ng/g) $\pm 2\sigma_m$	6.6	8.0 \pm 1.0	7.9	8.3 \pm 1.1	8.6	9.5 \pm 0.9	8.0	9.4 \pm 1.3	8.3 \pm 0.5	7.1 \pm 1.5	4.7	4.7 \pm 1.4	5.3 \pm 0.7	5.5 \pm 2.0	3.2 \pm 0.5

^aA&McD10—Arevalo and McDonough [2010]; J&O12—Jenner and O'Neill [2012]; Getal13—Gale et al. [2013]; W&K(2013)—White and Klein [2013]; Hof88—Hofmann [1988]; S&McD89—Sun and McDonough [1989]; S&S04—Salters and Stracke [2004].

^bModel compositions based on median and log-normal mean abundances of K, Th, and U measured in independent (and unfiltered) collections of global MORB.

^cG-MORB and N-MORB models of DMM composition assume 10% partial melting of the MORB source.

^dPropagated uncertainties assume $\pm 20\%$ (2σ) variations in models that do not explicitly report errors.

^eDMM compositional model based on the chemical and physical properties of abyssal peridotites derived by Workman and Hart [2005].

Table 6. Model Compositions for the Bulk Silicate Earth (BSE) Based on Geochemical and Geophysical Observations^a

Element	Traditional Geochemical Models						Enstatite Model	Collisional Erosion Model	Cosmochem BSE Model ^h	(Geo-) Dynamic BSE Model ^b		
	Jag79	Hof88	S&McD89	McD&S95 ^b	Jav99 ^{b,c}	P&O03					Lyb&K07	Geochem BSE Model ^d
K ($\mu\text{g/g} \pm 2\sigma$)	260	260	250	280 \pm 120	270 \pm 60	260 \pm 80	190 \pm 80	250 \pm 30	190 \pm 60	130 \pm 50	160 \pm 80	420 \pm 130
Th (ng/g) $\pm 2\sigma$	94	81	85	80 \pm 24	69 \pm 15	83 \pm 25	63 \pm 21	79 \pm 8	42 \pm 9	38 \pm 15	40 \pm 18	120 \pm 30
U (ng/g) $\pm 2\sigma$	26	20	21	20 \pm 8	20 \pm 4	22 \pm 7	17 \pm 6	21 \pm 2	14 \pm 3	10 \pm 4	12 \pm 5	30 \pm 8
Radioactive Heat (TW) $\pm 2\sigma$	24.1	20.5	21.0	20.5 \pm 7.5	19.0 \pm 4.2	21.3 \pm 6.4	16.3 \pm 5.8	20.4 \pm 2.1	12.5 \pm 3.0	9.9 \pm 3.7	11.2 \pm 5.0	30.9 \pm 8.0

^aJag79—Jagoutz [1979]; Hof88—Hofmann [1988]; S&McD89—Sun and McDonough [1989]; McD&S95—McDonough and Sun [1995]; Jav99—Javoy [1999]; P&O03—Palme and O'Neill [2003]; Lyb&K07—Lyubetskaya and Korenaga [2007]; O&P08—O'Neill and Palme [2008]; Jetal—Javoy et al. [2010].

^bK content and analytical uncertainty derived from the silicate Earth K/U ratio of 13,800 \pm 2600 (2σ) determined by Arevalo et al. [2009].

^cAnalytical uncertainties in K, Th, and U contents extrapolated from the reported uncertainty in the mantle Mg content of 22.5 \pm 5 (2σ) wt %.

^dPropagated uncertainties assume $\pm 20\%$ (2σ) variations in models that do not explicitly report errors.

^eK, Th and U contents calculated from the bulk Earth EH model, assuming negligible concentrations in the core.

^fAnalytical uncertainty of U content reflects 1.3 \pm 0.4 (2σ) $\mu\text{g/g}$ U in the continental crust [Rudnick and Gao, 2003] and uncertainties in the ⁴He flux of the modern mantle [Ozima and Podosek, 2002].

^gAnalytical uncertainties of Th and K contents are propagated assuming representative BSE ratios of Th/U = 3.8 \pm 0.4 (2σ) and K/U = 12,700 \pm 200 (2σ) from Jochum et al. [1983].

^hAverage K, Th, and U contents with propagated uncertainties of the enstatite BSE model of Javoy [1999] and the collisional erosion BSE model of O'Neill and Palme [2008].

Average Th and U contents and statistical uncertainties in the geophysical models of Turcotte and Schubert [1982, 2002] and Turcotte et al. [2001].

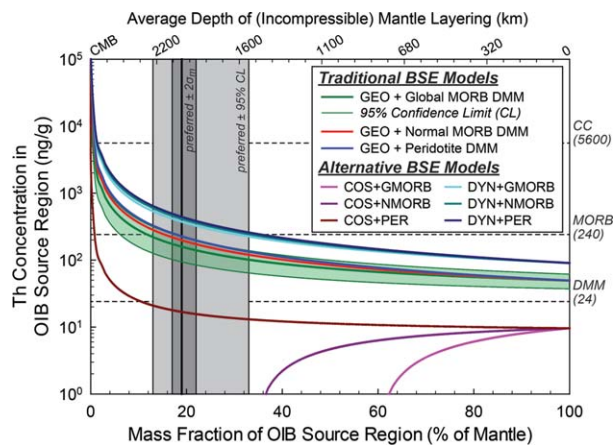


Figure 5. Relationship between the mass fraction and chemical enrichment of the OSR, which is dependent on the composition of the continental lithosphere (CL), source of MORB (or DMM) and the BSE following mass balance: $M^{BSE} X_{Th}^{BSE} = M^{CL} X_{Th}^{CL} + M^{DMM} X_{Th}^{DMM} + M^{OSR} X_{Th}^{OSR}$. The different mass balance curves consider three different flavors of DMM and BSE compositions, as listed in Tables 5 and 6, respectively. Curves that levy traditional geochemical models of the BSE are labeled as GEO and those that rely on cosmochemical and dynamical models are labeled as COS and DYN, respectively. The negative asymptotic trend lines (specifically COS+NMORB and COS+GMORB) indicate that these particular models require an OSR that is depleted in Th compared to the source of MORB in order to satisfy mass balance. [Color figure can be viewed in the online issue, which is available at wileyonlinelibrary.com.]

the MORB source region, the smaller and more enriched the OSR must be (Figure 5).

[31] Despite the large degree of a chemical variability observed in MORB derived from the Atlantic, Pacific, and Indian Ocean basins, the large quantity of accessible samples and abundance of data available publicly allow for a comprehensive evaluation of the composition of global MORB [e.g., Arevalo and McDonough, 2010; Jenner and O'Neill, 2012; Gale et al., 2013; White and Klein, 2013], and thus the DMM through inverse modeling. Alternative models of DMM composition that can be found in the literature are also reported in Table 5, including models based on the composition of lavas only with $(La/Sm)_N \leq 1.0$ (commonly deemed normal-type MORB, or N-MORB) [e.g., Hofmann, 1988; Sun and McDonough, 1989; Salters and Stracke, 2004] as well as those centered on the composition of abyssal peridotites, the residues of MORB source melting [Workman and Hart, 2005].

[32] Similarly, as shown in Table 6, there are multiple paradigms for the composition of the BSE.

Traditional geochemical models assume that the BSE follows CI chondritic relative proportions of refractory elements, with absolute abundances constrained by terrestrial samples [e.g., Jagoutz et al., 1979; Hofmann, 1988; Sun and McDonough, 1989; McDonough and Sun, 1995; Javoy, 1999; Palme and O'Neill, 2003; Lyubetskaya and Korenaga, 2007]. Alternative BSE models that rely on cosmochemical constraints include model compositions based on (1) enstatite chondrites, the only chondrite group with an O isotopic composition identical to the Earth [e.g., Javoy, 1999] and (2)

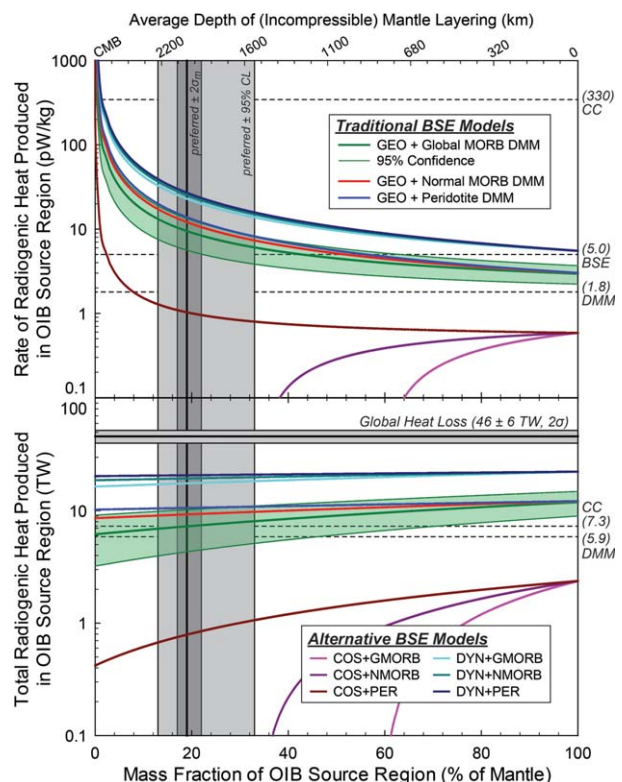


Figure 6. Interplay between the mass fraction of and radiogenic heat production within the OSR, which is dependent on the composition of the CL, DMM, and BSE, as described in Figure 5. Reference lines for the continental crust (CC) [Rudnick and Gao, 2003], DMM (based on the G-MORB model presented in Table 5), and BSE (based on the mean geochemical model presented in Table 6) are provided for comparison. The reference line for the total global heat loss (46 ± 6 TW, 2σ) is determined by Jaupart et al. [2007] and includes heat flux contributions from secular cooling, the planet's core, tidal dissipation, and gravitational energy. The negative asymptotic trend lines (specifically COS+NMORB and COS+GMORB) again indicate that these particular models require an OSR that is depleted in Th, and by extension radiogenic heat production, compared to the source of MORB in order to satisfy mass balance. [Color figure can be viewed in the online issue, which is available at wileyonlinelibrary.com.]

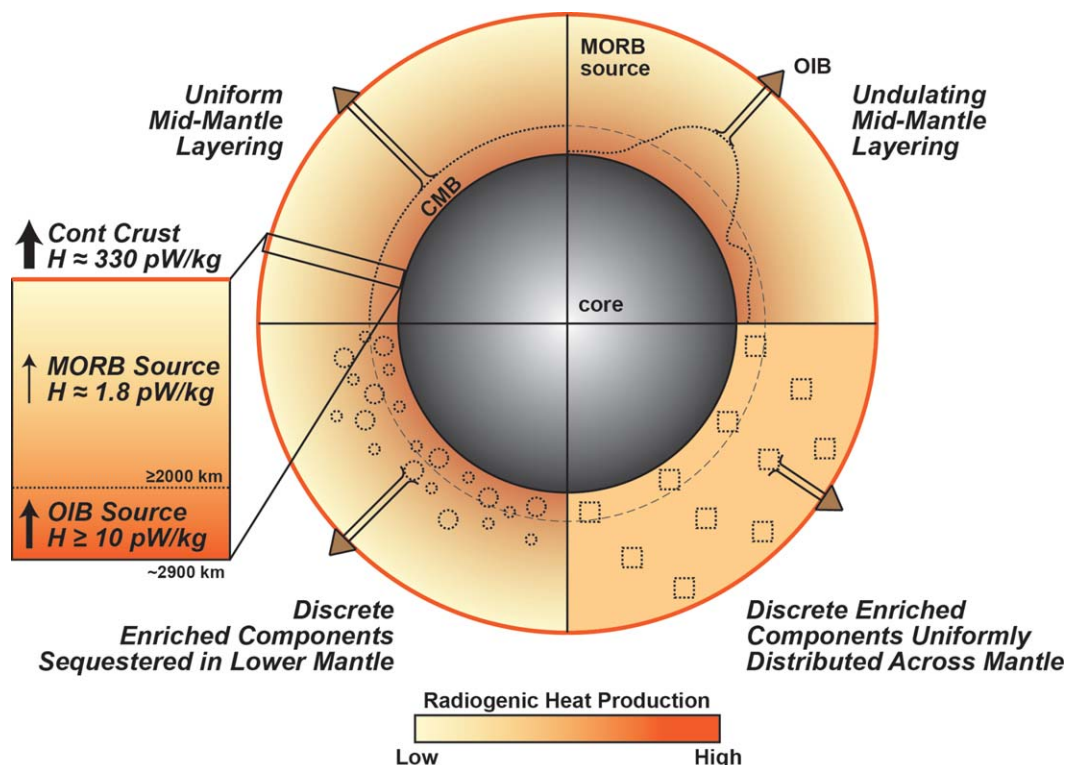


Figure 7. Schematic representation of plausible paradigms of mantle architecture, assuming only two distinct mantle source regions: the DMM and model OSR developed here. Regardless of whether the distinction between these two mantle reservoirs are preserved as a thermochemical stratification or blobs/blocks/streaks of OSR material suspended in a matrix of DMM, the preferred OIB source composition derived here indicates that the OSR represents approximately $\leq 19\%$ of the mass of the modern mantle, and contributes some 10 pW/kg of radiogenic heat (equating to 7.4 TW) to the planet's total surface heat loss. [Color figure can be viewed in the online issue, which is available at wileyonlinelibrary.com.]

net collisional erosion of approximately 10% silicate relative to metal during the Earth's accretion, and thus varying degrees of depletion of elements in the BSE according to their geochemical incompatibility [O'Neill and Palme, 2008]. Dynamical models require a BSE that is significantly more enriched in radioactive elements in order to satisfy calculations of the energetics of mantle convection, observed surface heat loss, and parameterized models of thermal evolution [e.g., Turcotte and Schubert, 1982, 2002; Turcotte et al., 2001].

[33] Despite the uncertainties introduced by these different models, we derive a range of prospective compositions/mass fractions of the OSR that satisfy the simple mass balance equation (equation (1)) described in section 1. As shown in Figure 5, our preferred model calculations take into account a DMM composition derived from a global MORB model (see Table 5) and a BSE composition averaged from a selection of traditional geochemical models (see Table 6). Our calculations

indicate that the OIB sources of the HIMU- and EM-type lavas analyzed here represents $\leq 19^{+3}_{-2}$ ($2\sigma_m$)% of the modern mantle by mass, with the remaining $\geq 81\%$ of the mantle represented by the DMM. If the mantle is described appropriately by a layered, two-component architecture (i.e., DMM + OSR), our model suggests that a thermochemical boundary layer exists at an average depth of $\geq 2000 \pm 100$ ($2\sigma_m$) km (assuming an incompressible mantle) or two thermochemical piles that extend up to midmantle levels. The potential for a sequestered or unsampled mantle reservoir, as inferred from trace element abundances [e.g., Rudnick et al., 2000], ^{146}Sm - ^{142}Nd isotopes [e.g., Boyet and Carlson, 2005], and rare gas systematics [e.g., Tolstikhin and Hofmann, 2005], would not change the compositional OIB source model presented here; rather, a tertiary mantle reservoir (such as an early enriched reservoir, or EER) would implicate a smaller (by mass) OSR and a larger DMM, according to the relationship:



$$M^{\text{BSE}} X_i^{\text{BSE}} = M^{\text{CL}} X_i^{\text{CL}} + M^{\text{DMM}} X_i^{\text{DMM}} + M^{\text{OSR}} X_i^{\text{OSR}} + M^{\text{EER}} X_i^{\text{EER}}, \quad (3)$$

where the mass and chemical enrichment of an EER with respect to element i are represented by M_i^{EER} and X_i^{EER} , respectively. For reference, M^{BSE} and M^{CC} are determined by Yoder [1995], X_i^{CL} is derived by Rudnick and Gao [2003], X_i^{BSE} and X_i^{DMM} are defined in Tables 5 and 6, and $M^{\text{OSR}} X_i^{\text{OSR}}$ is modeled here.

[34] The model calculations and uncertainties presented here take into account errors in the bivariate linear regression statistics in the Th versus MgO trends shown in Figures 2 and 3; these errors have been propagated into our estimated OIB parental melt and source compositions (see Table 4). Our preferred model also relies on a traditional geochemical model for the composition of the BSE with 79 ± 8 (2σ) ng/g Th (see Table 6), an estimated 24 ± 1 ng/g Th ($2\sigma_m$) in the DMM (see Table 5), and 5600 ± 1700 ng/g (2σ) Th in the CC [Rudnick and Gao, 2003].

[35] Regardless of whether or not the mantle is stratified, the OIB source compositions determined here have implications for the planet's radiogenic heat budget. As shown in Figures 6 and 7, our preferred model indicates that the rate of radiogenic heat produced within the OSR is on the order of 10 pW/kg, equating to some 7.3 TW of radiogenic heat produced in this mantle reservoir, assuming $C^{\text{OSR}}(\text{Th})/C^{\text{OSR}}(\text{U}) \approx 4.0$ and $C^{\text{OSR}}(\text{K})/C^{\text{OSR}}(\text{U}) \approx 10,400$ (average Th/U and K/U of lavas examined here, respectively). According to the traditional geochemical models reviewed here, 20.4 TW of radiogenic heat is produced by the BSE; therefore, approximately 5.9 TW of heat must be produced by the DMM, following mass balance and subtracting the 7.3 TW of radiogenic heat produced by the OIB source proposed here and the 7.2 TW of heat generated within the CL [Rudnick and Gao, 2003].

6. Conclusions

[36] Lavas from HIMU-type Cook-Austral and St. Helena islands, and EM-type Heard, Gough and Pitcairn Islands, Marquesas, Azores, Society and Samoa islands, all share similar parental melt compositions between 17 and 19 wt % MgO and averaging 2.1 ± 0.3 ($2\sigma_m$) $\mu\text{g/g}$ Th. Assuming the parental melts of the lavas examined here represent 5–10% partial melting of a peridotite, our model calculations suggest that these OIB are

derived from a hotspot source region with an average of 160 ± 20 ($2\sigma_m$) ng/g Th. The model OIB source composition determined here may represent a lower limit on the chemical enrichment and an upper limit on the mass fraction of the investigated end-member-type OIB sources, as we have assumed: melting of a dominantly peridotitic source lithology, and thus a lower production rate compared to melting of pyroxenite; and negligible dilution from the entrainment of depleted upper mantle materials during the ascent and emplacement of the lavas analyzed here. The potential for a tertiary “hidden” or unsampled mantle reservoir would only impact the relative mass fractions of the OSR and DMM and not the compositional model of the OSR presented here.

[37] Our calculations indicate that the mantle reservoir that serves as the source of the investigated end-member-type OIB must: (1) constitute some 19^{+3}_{-2} ($2\sigma_m$)% of the mantle by mass, equating to a potential thermochemical layering with an average depth of 2000 ± 100 ($2\sigma_m$) km (assuming an incompressible mantle) or two thermochemical piles that extend up to midmantle depths; and (2) contribute some 7.3 TW of radiogenic heat to the planet's total surface heat loss. Taking into account the 7.2 TW of radiogenic heat produced within the CL, the remaining 5.9 TW (equal to <2 pW/kg) of heat produced within the BSE must be supplied by the DMM. Thus, the hotspot source region that generates end-member OIB produces >5 times more radiogenic heat than the source of mid-ocean ridge volcanism, providing basal heating to the mantle, contributing to the energetics that drive mantle convection, and potentially supporting the formation of long-lived mantle plumes.

Acknowledgments

[38] We thank Bill White, Emily Klein, and an anonymous reviewer for their insightful comments regarding this work. This study was funded by NSF grant EAR-0739006 (to W.F.M.) and NSF CSEDI grant 0757808 (to R.J.W.).

References

- Allègre, C. J. (1968), Behavior of uranium-thorium-lead systems in upper mantle and model of mantle development during geological times, *Earth Planet. Sci. Lett.*, 5(4), 261–269.
Allègre, C. J., and D. L. Turcotte (1986), Implications of a two-component marble cake mantle, *Nature*, 323(6084), 123–127.



- Allègre, C. J., D. B. Othman, M. Polve, and P. Richard (1979), Nd-Sr isotopic correlation in mantle materials and geodynamic consequences, *Phys. Earth Planet. Inter.*, 19(4), 293–306.
- Allègre, C. J., T. Staudacher, P. Sarda, and M. Kurz (1983), Constraints on evolution of Earth's mantle from rare gas systematics, *Nature*, 303(5920), 762–766.
- Anderson, D. L. (2002), The case for irreversible chemical stratification of the mantle, *Int. Geol. Rev.*, 44(2), 97–116.
- Arevalo, R., Jr., and W. F. McDonough (2010), Chemical variations and regional diversity observed in MORB, *Chem. Geol.*, 271(1–2), 70–85.
- Arevalo, R., Jr., W. F. McDonough, and M. Luong (2009), The K/U ratio of the silicate Earth: Insights into mantle composition, structure and thermal evolution, *Earth Planet. Sci. Lett.*, 278(3–4), 361–369.
- Barling, J., S. L. Goldstein, and I. A. Nicholls (1994), Geochemistry of Heard Island (southern Indian Ocean): Characterization of an enriched mantle component and implications for enrichment of the sub-Indian Ocean mantle, *J. Petrol.*, 35(4), 1017–1053.
- Becker, T. W., J. B. Kellogg, and R. J. O'Connell (1999), Thermal constraints on the survival of primitive blobs in the lower mantle, *Earth Planet. Sci. Lett.*, 171(3), 351–365.
- Beier, C., A. Stracke, and K. M. Haase (2007), The peculiar geochemical signatures of Sao Miguel (Azores) lavas: Metasomatized or recycled mantle sources?, *Earth Planet. Sci. Lett.*, 259(1–2), 186–199.
- Bezous, A., and E. Humler (2005), The Fe³⁺/ΣFe ratios of MORB glasses and their implications for mantle melting, *Geochim. Cosmochim. Acta*, 69(3), 711–725.
- Boyet, M., and R. W. Carlson (2005), 142Nd evidence for early (>4.53 Ga) global differentiation of the silicate Earth, *Science*, 309(5734), 576–581.
- Breger, L., and B. Romanowicz (1998), Three-dimensional structure at the base of the mantle beneath the central Pacific, *Science*, 282(5389), 718–720.
- Caroff, M., R. C. Maury, J. Leterrier, J. L. Joron, J. Cotten, and G. Guille (1993), Trace element behavior in the alkali basalt-comenditic trachyte series from Mururoa Atoll, French Polynesia, *Lithos*, 30(1), 1–22.
- Caroff, M., H. Guillou, M. Lamiaux, R. C. Maury, G. Guille, and J. Cotten (1999), Assimilation of ocean crust by hawaiitic and mugearitic magmas: An example from Eiao (Marquesas), *Lithos*, 46(2), 235–258.
- Chen, C. H. (1988), Estimation of the degree of partial melting by (Na₂O+K₂O) and Al₂O₃/SiO₂ of basic magmas, *Chem. Geol.*, 71(4), 355–364.
- Dasgupta, R., M. G. Jackson, and C. T. A. Lee (2010), Major element chemistry of ocean island basalts: Conditions of mantle melting and heterogeneity of mantle source, *Earth Planet. Sci. Lett.*, 289(3–4), 377–392.
- Davaille, A. (1999), Simultaneous generation of hotspots and superswells by convection in a heterogeneous planetary mantle, *Nature*, 402(6763), 756–760.
- Davaille, A., M. Le Bars, and C. Carbonne (2003), Thermal convection in a heterogeneous mantle, *C. R. Geosci.*, 335(1), 141–156.
- DePaolo, D. J., and G. J. Wasserburg (1976), Inferences about magma sources and mantle structure from variations of 143Nd/144Nd, *Geophys. Res. Lett.*, 3, 743–746.
- Dupuy, C., H. G. Barseczus, J. M. Liotard, and J. Dostal (1988), Trace element evidence for the origin of ocean island basalts: An example from the Austral Islands (French Polynesia), *Contrib. Mineral. Petrol.*, 98(3), 293–302.
- Dupuy, C., H. G. Barseczus, J. Dostal, P. Vidal, and J. M. Liotard (1989), Subducted and recycled lithosphere as the mantle source of ocean island basalts from southern Polynesia, central Pacific, *Chem. Geol.*, 77(1), 1–18.
- Eggins, S. M. (1992), Petrogenesis of Hawaiian tholeiites: 2. Aspects of dynamic melt segregation, *Contrib. Mineral. Petrol.*, 110(2–3), 398–410.
- Feigenson, M. D., L. L. Bolge, M. J. Carr, and C. T. Herzberg (2003), REE inverse modeling of HSDP2 basalts: Evidence for multiple sources in the Hawaiian plume, *Geochem. Geophys. Geosyst.*, 4(2), 8706, doi:10.1029/2001GC000271.
- Forsyth, D. W., et al. (1998), Imaging the deep seismic structure beneath a mid-ocean ridge: The MELT experiment, *Science*, 280(5367), 1215–1218.
- Frey, F. A., D. H. Green, and S. D. Roy (1978), Integrated models of basalt petrogenesis: Study of quartz tholeiites to olivine melilitites from South Eastern Australia utilizing geochemical and experimental petrological data, *J. Petrol.*, 19(3), 463–513.
- Fukao, Y., M. Obayashi, H. Inoue, and M. Nenbai (1992), Subducting slabs stagnant in the mantle transition zone, *J. Geophys. Res. Solid Earth*, 97, 4809–4822.
- Fukao, Y., S. Widiyantoro, and M. Obayashi (2001), Stagnant slabs in the upper and lower mantle transition region, *Rev. Geophys.*, 39, 291–323.
- Gale, A., C. A. Dalton, C. H. Langmuir, Y. Su, and J.-G. Schilling (2013), The mean composition of ocean ridge basalts, *Geochem. Geophys. Geosyst.*, doi:10.1029/2012GC004334 in press.
- Garnero, E. J. (2000), Heterogeneity of the lowermost mantle, *Annu. Rev. Earth Planet. Sci.*, 28, 509–537.
- Gast, P. W. (1968), Trace element fractionation and origin of tholeiitic and alkaline magma types, *Geochim. Cosmochim. Acta*, 32(10), 1057–1086.
- Gast, P. W., C. Hedge, and G. R. Tilton (1964), Isotopic composition of lead and strontium from Ascension and Gough Islands, *Science*, 145(363), 1181–1185.
- Geist, D., W. M. White, F. Albarede, K. Harpp, R. Reynolds, J. Blichert-Toft, and M. Kurz (2003), Volcanic evolution in the Galapagos: The dissected shield of Volcan Ecuador, *Geochem. Geophys. Geosyst.*, 3(10), 1061, doi:10.1029/2002GC000355.
- Grand, S. P. (1994), Mantle shear structure beneath the Americas and surrounding oceans, *J. Geophys. Res. Solid Earth*, 99, 11,591–11,621.
- Grand, S. P. (2002), Mantle shear-wave tomography and the fate of subducted slabs, *Philos. Trans. R. Soc. A*, 360(1800), 2475–2491.
- Green, D. H. (1970), A review of experimental evidence on the origin of basaltic and nephelinitic magmas, *Phys. Earth Planet. Inter.*, 3, 221–235.
- Green, D. H., and A. E. Ringwood (1967), The genesis of basaltic magmas, *Contrib. Mineral. Petrol.*, 15(2), 103–190.
- Griffiths, R. W., and I. H. Campbell (1990), Stirring and structure in mantle starting plumes, *Earth Planet. Sci. Lett.*, 99(1–2), 66–78.
- Hanan, B. B., and Graham, D. W. (1996), Lead and helium isotope evidence from oceanic basalts for a common deep source of mantle plumes, *Science*, 272(5264), 991–995, doi:10.1126/science.272.5264.991.
- Hart, S. R. (1988), Heterogeneous mantle domains: Signatures, genesis and mixing chronologies, *Earth Planet. Sci. Lett.*, 90(3), 273–296.
- Hart, S. R., E. H. Hauri, L. A. Oschmann, and J. A. Whitehead (1992), Mantle plumes and entrainment/Isotopic evidence, *Science*, 256, 517–520.



- Hemond, C., C. W. Devey, and C. Chauvel (1994), Source compositions and melting processes in the Society and Austral plumes (South Pacific Ocean): Element and isotope (Sr, Nd, Pb, Th) geochemistry, *Chem. Geol.*, *115*(1-2), 7–45.
- Hirschmann, M. M., T. Kogiso, M. B. Baker, and E. M. Stolper (2003), Alkalic magmas generated by partial melting of garnet pyroxenite, *Geology*, *31*(6), 481–484.
- Hofmann, A. W. (1988), Chemical differentiation of the Earth: The relationship between mantle, continental crust and oceanic crust, *Earth Planet. Sci. Lett.*, *90*(3), 297–314.
- Hofmann, A. W. (2003), Sampling mantle heterogeneity through oceanic basalts: Isotopes and trace elements, in *The Mantle and Core*, edited by R. W. Carlson, pp. 61–101, Elsevier-Pergamon, Oxford, U.K.
- Hofmann, A. W., and W. M. White (1982), Mantle plumes from ancient oceanic crust, *Earth Planet. Sci. Lett.*, *57*(2), 421–436.
- Hofmann, A. W., K. P. Jochum, M. Seufert, and W. M. White (1986), Nb and Pb in oceanic basalts: New constraints on mantle evolution, *Earth Planet. Sci. Lett.*, *79*(1-2), 33–45.
- Honda, M., I. Mcdougall, D. B. Patterson, A. Doulgeris, and D. A. Clague (1991), Possible solar noble-gas component in Hawaiian basalts, *Nature*, *349*(6305), 149–151.
- Huang, S., and F. A. Frey (2003), Trace element abundances of Mauna Kea basalt from phase 2 of the Hawaii Scientific Drilling Project: Petrogenetic implications of correlations with major element content and isotopic ratios, *Geochem. Geophys. Geosyst.*, *4*(6), 8711, doi:10.1029/2002GC000322.
- Ireland, T. J., R. Arevalo, R. J. Walker, and W. F. McDonough (2009), Tungsten in Hawaiian picrites: A compositional model for the sources of Hawaiian lavas, *Geochim. Cosmochim. Acta*, *73*(15), 4517–4530.
- Jagoutz, E., H. Palme, H. Baddenhausen, K. Blum, M. Cendales, G. Dreibus, B. Spettel, V. Lorenz, and H. Wanke (1979), The abundances of major, minor and trace elements in the Earth's mantle as derived from primitive ultramafic nodules, *Proc. Lunar Sci. Conf. 10th*, *2*, 2031–2050.
- Jaques, A. L., and D. H. Green (1980), Anhydrous melting of peridotite at 0–15 kb pressure and the genesis of tholeiitic basalts, *Contrib. Mineral. Petrol.*, *73*(3), 287–310.
- Jaupart, C., S. Labrosse, and J.-C. Mareschal (2007), Temperatures, heat and energy in the mantle of the Earth, in *Mantle Convection*, edited by D. Bercovici, vol. 7, pp. 253–303, Elsevier-Pergamon, Oxford, U.K.
- Javoy, M. (1999), Chemical earth models, *C. R. Acad. Sci. Ser. II*, *329*(8), 537–555.
- Jenner, F. E., and H. S. O'Neill (2012), Analysis of 60 elements in 616 ocean floor basaltic glasses, *Geochem. Geophys. Geosyst.*, *13*, Q02005, doi:10.1029/2011GC004009.
- Johnson, K. T. M., H. J. B. Dick, and N. Shimizu (1990), Melting in the oceanic upper mantle: An ion microprobe study of diopsides in abyssal peridotites, *J. Geophys. Res. Solid Earth*, *95*, 2661–2678.
- Kalfoun, F. (2001), Geochemie du niobium et du tantalé: Distribution et fractionnement de ces deux éléments dans les différents réservoirs terrestres, Thèse de Docteur de L Université Montpellier II, Acad. de Montpellier, Montpellier, France.
- Kárason, H., and R. D. van der Hilst (2000), Constraints on mantle convection from seismic tomography, in *The History and Dynamics of Global Plate Motions*, *Geophys. Monogr. Ser.*, vol. 121, edited by M. A. Richards, R. G. Gordon, and R. D. van der Hilst, pp. 277–288, AGU, Washington, D. C.
- Kellogg, L. H., B. H. Hager, and R. D. van der Hilst (1999), Compositional stratification in the deep mantle, *Science*, *283*(5409), 1881–1884.
- Klein, E. M., and C. H. Langmuir (1987), Global correlations of ocean ridge basalt chemistry with axial depth and crustal thickness, *J. Geophys. Res.*, *92*, 8089–8115.
- Klemme, S., J. D. Blundy, and B. J. Wood (2002), Experimental constraints on major and trace element partitioning during partial melting of eclogite, *Geochim. Cosmochim. Acta*, *66*(17), 3109–3123.
- Koornneef, J. M., A. Stracke, B. Bourdon, and K. Gronvold (2012), The influence of source heterogeneity on the U-Th-Pa-Ra disequilibria in post-glacial tholeiites from Iceland, *Geochim. Cosmochim. Acta*, *87*, 243–266.
- Kumagai, I. (2002), On the anatomy of mantle plumes: Effect of the viscosity ratio on entrainment and stirring, *Earth Planet. Sci. Lett.*, *198*(1-2), 211–224.
- Kurz, M. D., W. J. Jenkins, J. G. Schilling, and S. R. Hart (1982), Helium isotopic variations in the mantle beneath the Central North Atlantic Ocean, *Earth Planet. Sci. Lett.*, *58*(1), 1–14.
- Langmuir, C. H., J. F. Bender, A. E. Bence, G. N. Hanson, and S. R. Taylor (1977), Petrogenesis of basalts from the FAMOUS Area: Mid-Atlantic Ridge, *Earth Planet. Sci. Lett.*, *36*(1), 133–156.
- Lin, S. C., and P. E. van Keken (2006), Deformation, stirring and material transport in thermochemical plumes, *Geophys. Res. Lett.*, *33*, L20306, doi:10.1029/2006GL027037.
- Liotard, J. M., and H. G. Barszczus (1985), Contribution à la connaissance pétrographique et géochimique des îlots marotiri, Polynésie française (Océan Pacifique centre-Sud), *C. R. Acad. Sci.*, *301*(9), 611–614.
- Liotard, J. M., R. C. Maury, and H. G. Barszczus (1990), La diversité des basaltes en Polynésie française: Approche minéralogique, *Géodynamique*, *5*(2), 121–134.
- Lyubetskaya, T., and J. Korenaga (2007), Chemical composition of Earth's primitive mantle and its variance: 1. Method and results, *J. Geophys. Res. Solid Earth*, *112*, B03212, doi:10.1029/2005JB004224.
- Maaløe, S., and R. B. Pedersen (2003), Two methods for estimating the degree of melting and trace element concentrations in the sources of primary magmas, *Chem. Geol.*, *193*, 155–166.
- Masters, G., G. Laske, H. Bolton, and A. Dziewonski (2000), The relative behavior of shear velocity, bulk sound speed, and compressional velocity in the mantle: Implications for chemical and thermal structure, in *Earth's Deep Interior*, *AGU Monogr. Ser.*, vol. 117, edited by S. Karato, pp. 63–87, AGU, Washington, D. C.
- Maury, R. C., R. Andriambololona, and C. Dupuy (1978), Evolution comparée de deux séries alcalines du Pacifique Central: Rôle de la fugacité d'oxygène et de la pression d'eau, *Bull. Volcanol.*, *41*(2), 97–118.
- McDonough, W. F., and S. S. Sun (1995), The composition of the Earth, *Chem. Geol.*, *120*(3-4), 223–253.
- McKenzie, D., and M. J. Bickle (1988), The volume and composition of melt generated by extension of the lithosphere, *J. Petrol.*, *29*(3), 625–679.
- McNamara, A. K., and S. J. Zhong (2005), Thermochemical structures beneath Africa and the Pacific Ocean, *Nature*, *437*(7062), 1136–1139.
- Minster, J. F., and C. J. Allègre (1978), Systematic use of trace elements in igneous processes: 3. Inverse problem of batch partial melting in volcanic suites, *Contrib. Mineral. Petrol.*, *68*(1), 37–52.
- Montelli, R., G. Nolet, F. A. Dahlen, G. Masters, E. R. Engdahl, and S. H. Hung (2004), Finite-frequency tomography reveals a variety of plumes in the mantle, *Science*, *303*(5656), 338–343.



- Morgan, J. P., and W. J. Morgan (1999), Two-stage melting and the geochemical evolution of the mantle: A recipe for mantle plum-pudding, *Earth Planet. Sci. Lett.*, 170(3), 215–239.
- Neavel, K. E., and A. M. Johnson (1991), Entrainment in compositionally buoyant plumes, *Tectonophysics*, 200, 1–15.
- Ni, S. D., E. Tan, M. Gurnis, and D. Helmlinger (2002), Sharp sides to the African superplume, *Science*, 296(5574), 1850–1852.
- Nisbet, E. G., and J. A. Pearce (1977), Clinopyroxene composition in mafic lavas from different tectonic settings, *Contrib. Mineral. Petrol.*, 63(2), 149–160.
- Niu, Y. L. (1997), Mantle melting and melt extraction processes beneath ocean ridges: Evidence from abyssal peridotites, *J. Petrol.*, 38(8), 1047–1074.
- Niu, Y. L., and M. J. O'Hara (2003), Origin of ocean island basalts: A new perspective from petrology, geochemistry, and mineral physics considerations, *J. Geophys. Res. Solid Earth*, 108(B4), 2209, doi:10.1029/2002JB002048.
- Norman, M. D., and M. O. Garcia (1999), Primitive magmas and source characteristics of the Hawaiian plume: Petrology and geochemistry of shield picrites, *Earth Planet. Sci. Lett.*, 168(1-2), 27–44.
- Norman, M. D., M. O. Garcia, V. S. Kamenetsky, and R. L. Nielsen (2002), Olivine-hosted melt inclusions in Hawaiian picrites: Equilibration, melting, and plume source characteristics, *Chem. Geol.*, 183(1-4), 143–168.
- O'Neill, H. S. C., and H. Palme (2008), Collisional erosion and the non-chondritic composition of the terrestrial planets, *Philos. Trans. R. Soc. A*, 366(1883), 4205–4238.
- O'Nions, R. K., N. M. Evensen, and P. J. Hamilton (1979), Geochemical modeling of mantle differentiation and crustal growth, *J. Geophys. Res.*, 84, 6091–6101.
- Palme, H., and H. S. C. O'Neill (2003), Cosmochemical estimates of mantle composition, in *The Mantle and Core*, edited by R. W. Carlson, pp. 1–38, Elsevier-Pergamon, Oxford.
- Pertermann, M., and M. M. Hirschmann (2003), Partial melting experiments on a MORB-like pyroxenite between 2 and 3 GPa: Constraints on the presence of pyroxenite in basalt source regions from solidus location and melting rate, *J. Geophys. Res. Solid Earth*, 108(B2), 2125, doi:10.1029/2000JB000118.
- Pertermann, M., M. M. Hirschmann, K. Hametner, D. Gunther, and M. W. Schmidt (2004), Experimental determination of trace element partitioning between garnet and silica-rich liquid during anhydrous partial melting of MORB-like eclogite, *Geochem. Geophys. Geosyst.*, 5(5), Q05A01, doi:10.1029/2003GC000638.
- Prytulak, J., and T. Elliott (2007), TiO₂ enrichment in ocean island basalts, *Earth Planet. Sci. Lett.*, 263(3-4), 388–403.
- Prytulak, J., and T. Elliott (2009), Determining melt productivity of mantle sources from U-238-Th-230 and U-235-Pa-231 disequilibria; an example from Pico Island, Azores, *Geochim. Cosmochim. Acta*, 73(7), 2103–2122.
- Putirka, K. D. (2005), Mantle potential temperatures at Hawaii, Iceland, and the mid-ocean ridge system, as inferred from olivine phenocrysts: Evidence for thermally driven mantle plumes, *Geochem. Geophys. Geosyst.*, 6, Q05L08, doi:10.1029/2005GC000915.
- Putirka, K. (2008), Excess temperatures at ocean islands: Implications for mantle layering and convection, *Geology*, 36(4), 283–286.
- Rhodes, J. M., and M. J. Vollinger (2005), Ferric/ferrous ratios in 1984 Mauna Loa lavas: a contribution to understanding the oxidation state of Hawaiian magmas, *Contrib. Mineral. Petrol.*, 149(6), 666–674.
- Ritsema, J., H. J. van Heijst, and J. H. Woodhouse (1999), Complex shear wave velocity structure imaged beneath Africa and Iceland, *Science*, 286(5446), 1925–1928.
- Ritsema, J., H. J. van Heijst, and J. H. Woodhouse (2004), Global transition zone tomography, *J. Geophys. Res.*, 109, B02302, doi:10.1029/2003JB002610.
- Roeder, P. L., and R. F. Emslie (1970), Olivine-liquid equilibrium, *Contrib. Mineral. Petrol.*, 29(4), 275–289.
- Rudnick, R. L., and S. Gao (2003), Composition of the continental crust, in *The Crust*, vol. 3, edited by R. L. Rudnick, pp. 1–64, Elsevier-Pergamon, Oxford, U. K.
- Rudnick, R. L., M. Barth, I. Horn, and W. F. McDonough (2000), Rutile-bearing refractory eclogites: Missing link between continents and depleted mantle, *Science*, 287(5451), 278–281.
- Salters, V. J. M., and J. Longhi (1999), Trace element partitioning during the initial stages of melting beneath mid-ocean ridges, *Earth Planet. Sci. Lett.*, 166(1-2), 15–30.
- Salters, V. J. M., and A. Stracke (2004), Composition of the depleted mantle, *Geochem. Geophys. Geosyst.*, 5(5), Q05B07, doi:10.1029/2003GC000597.
- Salters, V. J. M., J. E. Longhi, and M. Bizimis (2002), Near mantle solidus trace element partitioning at pressures up to 3.4 GPa, *Geochem. Geophys. Geosyst.*, 3(7), 2002, doi:10.1029/2001GC000148.
- Schilling, J. G. (1973), Iceland mantle plume: Geochemical study of Reykjanes Ridge, *Nature*, 242(5400), 565–571.
- Shaw, D. M. (1970), Trace element fractionation during anatexis, *Geochim. Cosmochim. Acta*, 34(2), 237–243.
- Sims, K. W. W., D. J. Depaolo, M. T. Murrell, W. S. Baldrige, S. J. Goldstein, and D. A. Clague (1995), Mechanisms of magma generation beneath Hawaii and mid-ocean ridges: Uranium/thorium and samarium/neodymium isotopic evidence, *Science*, 267(5197), 508–512.
- Sims, K. W. W., D. J. DePaolo, M. T. Murrell, W. S. Baldrige, S. Goldstein, D. Clague, and M. Jull (1999), Porosity of the melting zone and variations in the solid mantle upwelling rate beneath Hawaii: Inferences from 238U-230Th-226Ra and 235U-231Pa disequilibria, *Geochim. Cosmochim. Acta*, 63(23-24), 4119–4138.
- Spiegelman, M., and P. Kenyon (1992), The requirements for chemical disequilibrium during magma migration, *Earth Planet. Sci. Lett.*, 109(3-4), 611–620.
- Stracke, A., and B. Bourdon (2009), The importance of melt extraction for tracing mantle heterogeneity, *Geochim. Cosmochim. Acta*, 73(1), 218–238.
- Stracke, A., A. Zindler, V. J. M. Salters, D. McKenzie, J. Blichert-Toft, F. Albarede, and K. Gronvold (2003), Theistareykir revisited, *Geochem. Geophys. Geosyst.*, 4(2), 8507, doi:10.1029/2001GC000201.
- Stracke, A., A. W. Hofmann, and S. R. Hart (2005), FOZO, HIMU, and the rest of the mantle zoo, *Geochem. Geophys. Geosyst.*, 6, 8507, doi:10.1029/2001GC000201.
- Stracke, A., B. Bourdon, and D. McKenzie (2006), Melt extraction in the Earth's mantle: Constraints from U-Th-Pa-Ra studies in oceanic basalts, *Earth Planet. Sci. Lett.*, 244(1-2), 97–112.
- Su, W. J., R. L. Woodward, and A. M. Dziewonski (1994), Degree-12 model of shear velocity heterogeneity in the mantle, *J. Geophys. Res. Solid Earth*, 99, 6945–6980.
- Sun, S. S., and G. N. Hanson (1975), Origin of Ross Island basanitoids and limitations upon heterogeneity of mantle sources for alkali basalts and nephelinites, *Contrib. Mineral. Petrol.*, 52(2), 77–106.
- Sun, S. S., and W. F. McDonough (1989), Chemical and isotopic systematics of oceanic basalts: Implications for mantle



- composition and processes, in *Magmatism in the Ocean Basins*, edited by A. D. Saunders and M. J. Norry, pp. 313–345, *Geol. Soc. Spec. Publ.* London, 42, 313–345.
- Tackley, P. J. (1998), Three-dimensional simulations of mantle convection with a thermo-chemical basal boundary layer: D1? in *The Core-Mantle Boundary Region*, *Geophys. Monogr. Ser.*, vol. 28, edited by M. Gurnis, et al., pp. 231–253, AGU, Washington, D. C.
- Tatsumoto, M. (1978), Isotopic composition of lead in oceanic basalt and its implication to mantle evolution, *Earth Planet. Sci. Lett.*, 38(1), 63–87.
- Tolstikhin, I., and A. W. Hofmann (2005), Early crust on top of the Earth's core, *Phys. Earth Planet. Inter.*, 148(2-4), 109–130.
- Trampert, J., F. Deschamps, J. Resovsky, and D. Yuen (2004), Probabilistic tomography maps chemical heterogeneities throughout the lower mantle, *Science*, 306(5697), 853–856.
- Treuil, M., and J. L. Joron (1975), Utilisation des 'éléments hydromagmatophiles pour la simplification de la modélisation quantitative des processus magmatiques. Exemples des L'Afar et de la Dorsale Médiatlantique, *Soc. Ital. Mineral. Petrol.*, 31, 125–174.
- Turcotte, D. L., and G. Schubert (1982), *Geodynamics: Applications of Continuum Physics to Geological Problems*, Wiley, New York.
- Turcotte, D. L., and G. Schubert (2002), *Geodynamics*, 2nd ed., Cambridge Univ. Press, New York.
- Turcotte, D. L., D. Paul, and W. M. White (2001), Thorium-uranium systematics require layered mantle convection, *J. Geophys. Res. Solid Earth*, 106, 4265–4276.
- van der Hilst, R., R. Engdahl, W. Spakman, and G. Nolet (1991), Tomographic imaging of subducted lithosphere below Northwest Pacific island arcs, *Nature*, 353(6339), 37–43.
- van der Hilst, R. D., and H. Kárason (1999), Compositional heterogeneity in the bottom 1000 kilometers of Earth's mantle: Toward a hybrid convection model, *Science*, 283(5409), 1885–1888.
- van der Hilst, R. D., S. Widiyantoro, and E. R. Engdahl (1997), Evidence for deep mantle circulation from global tomography, *Nature*, 386(6625), 578–584.
- van Keken, P. (1997), Evolution of starting mantle plumes: A comparison between numerical and laboratory models, *Earth Planet. Sci. Lett.*, 148(1-2), 1–11.
- van Keken, P. E., E. H. Hauri, and C. J. Ballentine (2002), Mantle mixing: The generation, preservation, and destruction of chemical heterogeneity, *Annu. Rev. Earth Planet. Sci.*, 30, 493–525.
- Vidale, J. E., G. Schubert, and P. S. Earle (2001), Unsuccessful initial search for a midmantle chemical boundary with seismic arrays, *Geophys. Res. Lett.*, 28, 859–862.
- Wang, Y., and L. X. Wen (2004), Mapping the geometry and geographic distribution of a very low velocity province at the base of the Earth's mantle, *J. Geophys. Res.*, 109, B10305, doi:10.1029/2003JB002674.
- Watson, S., and D. McKenzie (1991), Melt generation by plumes: A study of Hawaiian volcanism, *J. Petrol.*, 32(3), 501–537.
- Weaver, B. L. (1991), The origin of ocean island basalt end-member compositions: Trace-element and isotopic constraints, *Earth Planet. Sci. Lett.*, 104(2-4), 381–397.
- Wen, L. X., and D. L. Anderson (1995), The fate of slabs inferred from seismic tomography and 130 million years of subduction, *Earth Planet. Sci. Lett.*, 133(1-2), 185–198.
- White, W. M. (1985), Sources of oceanic basalts: Radiogenic isotopic evidence, *Geology*, 13(2), 115–118.
- White, W. M., and E. M. Klein (2013), The oceanic crust, in *The Crust*, vol. 4., edited by R. L. Rudnick, Elsevier-Perгамon, Oxford, U. K., in press.
- Willbold, M., and K. P. Jochum (2005), Multi-element isotope dilution sector field ICP-MS: A precise technique for the analysis of geological materials and its application to geological reference materials, *Geostand. Geoanal. Res.*, 29(1), 63–82.
- Willbold, M., and A. Stracke (2006), Trace element composition of mantle end-members: Implications for recycling of oceanic and upper and lower continental crust, *Geochem. Geophys. Geosyst.*, 7, Q04004, doi:10.1029/2005GC001005.
- Workman, R. K., and S. R. Hart (2005), Major and trace element composition of the depleted MORB mantle (DMM), *Earth Planet. Sci. Lett.*, 231(1-2), 53–72.
- Workman, R. K., S. R. Hart, M. Jackson, M. Regelous, K. A. Farley, J. Blusztajn, M. Kurz, and H. Staudigel (2004), Recycled metasomatized lithosphere as the origin of the enriched mantle II (EM2) end-member: Evidence from the Samoan volcanic chain, *Geochem. Geophys. Geosyst.*, 5(4), Q04008, doi:10.1029/2003GC000623.
- Yaxley, G. M. (2000), Experimental study of the phase and melting relations of homogeneous basalt plus peridotite mixtures and implications for the petrogenesis of flood basalts, *Contrib. Mineral. Petrol.*, 139(3), 326–338.
- Yoder, C. F. (1995), Astrometric and geodetic properties of Earth and the Solar System, in *Global Earth Physics: A Handbook of Physical Constants*, vol. 1, edited by T. J. Ahrens, pp. 1–31, AGU, Washington, D. C.
- Zhao, D. (2001), Seismic structure and origin of hotspots and mantle plumes, *Earth Planet. Sci. Lett.*, 192(3), 251–265.
- Zhou, H. W., and R. W. Clayton (1990), P and s-wave travel time inversions for subducting slab under the island arcs of the northwest Pacific, *J. Geophys. Res. Solid Earth*, 95, 6829–6851.
- Zindler, A., and S. Hart (1986), Chemical geodynamics, *Annu. Rev. Earth Planet. Sci.*, 14, 493–571.
- Zindler, A., E. Jagoutz, and S. Goldstein (1982), Nd, Sr and Pb isotopic systematics in a 3-component mantle: A new perspective, *Nature*, 298(5874), 519–523.